Homogenization
of strongly heterogeneous porous media

Thesis of the dissertation
submitted to the Czech Academy of Sciences

•

March 9, 2011

Eduard Rohan

Department of Mechanics, Faculty of Applied Sciences,
University of West Bohemia in Pilsen,
Univerzitní 22, 30614 Plzeň, Czech Republic
E-mail: rohan@kme.zcu.cz

Resumé

Homogenization techniques were developed to *simplify* description and modeling of heterogeneous structures where the characteristic size of the heterogeneities is much smaller than the size of the whole structure. Usually the *simplification* is associated with tractability of numerical modeling: "original structures", like fiber composites, or masonry are constructed by repeating some heterogeneity patterns which are related to oscillation of material coefficients. Therefore, the "direct modeling approach", where all the oscillations must be captured, may lead to extremely large "discretized" models with untractable numbers of equations to be solved. The homogenization-based analysis and numerical modeling is based on computing effective material properties characterizing the heterogeneity patterns. Thus, in contrast with the "original" models with oscillating material parameters, the "homogenized models" are characterized by "constant" effective material coefficients, so that the number of equations obtained by the discretization is reduced by several orders.

However, the "simplification" in the context of a reduced size of matrices featuring the numerical model does not mean *necessarily* that the homogenized model is simpler in its structure than the original one. When more complex heterogeneous continua are considered, where *qualitatively* different phases interact at the "microscopic level", the homogenization results in qualitatively new models which differ in their structure from any of the models describing the particular phases. In this way, *new constitutive laws* can be obtained, characterized by effective material parameters with very clear physical explanation. This is a great advantage of the homogenization-based modeling which cannot be achieved easily by phenomenological approaches. What makes the homogenization working better is the geometry and topology of the microstructure which is transformed into the effective material coefficients by means of solving so-called "microscopic problems". This is demonstrated on several problems studied in the DISSERTATION .

The *high-contrast media* and *thin structures*, which both are in the focus of the DISSERTATION , present a special example of combining qualitatively different media. The adjectives "high" and "thin" are to be understood in the sense of *material scaling*: the idea is to study mathematical models where the coefficients of the partial differential equations associated with one of the phases depend on the characteristic size ε of the microstructure, thereby strong heterogeneities are produced. This modeling approach was applied to study waves in two-phase elastic composites with "weak" inclusions, where the elasticity is scaled by ε^2, or to describe poroelastic behaviour in double-porous media, where the scaling is a natural consequence of velocity profiles in pores of the dual porosity. For homogenization of thin structures the scaling is related to the thickness, which leads to reduced spatial dimension of the problem.

These issues form the spine-bone of the DISSERTATION which is presented as a collection of papers. They can be associated with one of the main themes: 1) wave propagation in strongly heterogeneous solids, 2) perfusion in double-porous fluid-saturated media. Few papers are devoted to the sensitivity analysis for optimal design of periodic microstructures. All problems treated here by the homogenization are linear, or linearized, which allows for

decoupling the so-called limit two-scale problems into the macroscopic and microscopic ones.

The following topics are studied by homogenization methods:

- piezoelectric-elastic composites, [9, 21],

- waves in phononic crystals – elastic, or piezo-elastic high contrast composites, [1, 24, 22, 3, 4, 7],

- acoustic waves and transmission on thin (rigid) sieves, acoustic fluid in layers containing obstacles, [20, 7],

- electromagnetic waves and transmission through heterogeneous dielectric layers, [7],

- sensitivity analysis of homogenized coefficients for optimization of piezoelectric-elastic composites, [21],

- sensitivity analysis of band gaps for optimization of phononic materials, [23, 22, 21],

- sensitivity analysis of acoustic field for optimization of design of perforation (the sieve in acoustic fluid), [18],

- Biot compressible medium – fluid saturated porous material (FSPM) with double porosity, two-compartment model, application to bone poroelasticity, [5, 6, 15, 25],

- Biot incompressible medium – FSPM with double porosity, three-compartment model, application to perfusion in deforming tissue, [12, 16],

- large-deforming FSPM with fluid inclusions, application to smooth muscle tissue, [13, 10, 11, 8]

- large-deforming FSPM with double-porosity, application to perfusion, [19],

- Darcy flow in double-porous layer, application to perfusion, [14].

The work presented combines the theory of homogenization with its application to the particular problems and concerns also some numerical issues related to the computational homogenization-based multiscale modeling; it consists of three main steps: 1) solving local problems for characteristic "microscopic" responses and evaluation of homogenized (effective) material parameters, 2) solving the "macroscopic" problem with the effective parameters to obtain a global solution, 3) reconstruction of quantities of interest (e.g. stress, seepage flow) at the microscopic level for a selected macroscopic position. The last step combines the global response with the local characteristic response and presents the power of the multiscale modeling.

Acknowledgment

I am very grateful to Prof. Ing. Josef Rosenberg, DrSc. and Prof. RNDr. Pavel Drábek, DrSc. who encouraged me to complete this dissertation and provided me an indispensable moral support over the years of my appointment at the Faculty of Applied Sciences of the University of West Bohemia. Then I want to thank my colleagues Ing. Robert Cimrman, Ph.D. and Ing. Vladimír Lukeš, Ph.D. who implemented some of the models in their in-house developed finite element codes.

Především chci poděkovat mým nejbližším
za stálou morální podporu, pochopení a vlídné zázemí.

Contents

1 Introduction

This thesis summarizes author's contributions to the two-scale modeling of heterogeneous media using the homogenization method which is based upon asymptotic analysis of continuum models describing "periodic microstructures".

In the context of material modeling, the notion of homogenization is related usually to some approximate treatment of heterogeneous continua designed as mixtures of different constituents. The differences concern just values of the material parameters, or they are more substantial – for instance mixtures of fluid and solid components are considered. In the mechanical community, the homogenization is often understood in the sense of various averaging techniques based on definition of the RVE, the reference volume element. The RVE (small enough, but also sufficiently large) is subject to special loadings and the structural responses allow to compute the effective parameters characterizing the material behaviour. Apart of this averaging technique, there is the Eshelby theory which can describe behaviour of composites with elliptic inclusions which do not affect each other, being sparsely distributed at long distances.

The homogenization we have in mind is based on the asymptotic analysis of partial differential equations describing the continuum behaviour, whereby the small parameter describing the "microstructure size" influences space variation of the equation coefficients. We focus on problems characterized by strong heterogeneities — *large contrasts* in material coefficients; it is shown how the large contrast pronounced by its relationship with the scale may lead to "limit behaviour" which is qualitatively completely different from the one characterizing the original constituents.

Nowadays there exist several methods which allow one to obtain a model of homogenized continuum, i.e. by studying asymptotic behaviour of partial differential equations (PDEs) which governs a given problem characterized by the scale ε. The **periodic unfolding** which has been introduced and employed within the homogenization community recently, [CDG08], is relatively easy to use for linear, or quasi-linear problems. It presents a powerful tool for homogenization of locally periodic media even for those who have merely a little training in functional analysis.

Terminology. Although the notions like scale, or microstructure ale commonly understood, they may have different meaning depending on the particular context. Therefore, in Section 1 of the DISSERTATION we give a brief explanation of the following notions: structure of a medium, periodic / almost periodic structure, microstructure and microscopic level, scale. There is explained also some technical terminology which is referred to frequently throughout the text: representative periodic cell (RPC), Y-periodic function, corrector (basis) function, local and global problems.

Challenges and limitations. The asymptotic analysis of heterogeneous media provides a modeling tool which enables to retain important features of the structure (or microstructure) while reducing complexity of the problem in its primary setting. Periodi-

cally distributed structural details inducing some fluctuations of the physical fields can be condensed into the homogenized coefficients of the limit macroscopic (i.e. homogenized) model. Its numerical discretization leads to a computationally tractable problem which can be solved much cheaper than the original problem discretized with enormously large numbers of degrees of freedom, such that a huge computational power would be required to obtain a solution. Obviously, the benefits of "simplified" models obtained by homogenization is even more challenging when inverse problems are treated, like optimal design of the material structure.

However, the homogenized models describe the asymptotic behaviour, so that the limit behaviour is just an approximation of the reality which corresponds to a given scale $\varepsilon_0 > 0$. Apparently, the approximation becomes more accurate with decreasing ε_0, i.e. when the macroscopic structure involves more and more repeating microstructural periods.

Once the global response is known, having solved the macroscopic problem, the detail fluctuating response at the microscopic level can be computed for a given macroscopic position x. This procedure is often called the *microscopic response recovery* and is based on the *corrector functions*. They are obtained by combining the macroscopic solution at x with the local *corrector basis functions*. Thus, also the gradients of the quantity of interest can be obtained, like strains, stresses, or seepage velocities in porous media.

Models with scale-dependent parameters, like models of large contrast composites as an example, may amplify some special effects when passing to the limit with $\varepsilon \to 0$. For instance, limit model of the high contrast elasticity medium exhibits the dispersive behaviour, although the standard composites lead to a nondispersive medium which, in the limit, is characterized by the homogenized elasticity and by the mean-value of the density. In contrast, the ε^2-scaling of the elasticity coefficients in one of the composite constituents results in a frequency-dependent homogenized mass coefficients, hence the wave dispersion is obtained even in the limit $\varepsilon \to 0$.

It is worth to note that the standard homogenized model of composites preserve the homogeneous medium when all the constituents are identical, i.e. homogenization of a homogeneous material results in the same material. This is not possible, in principle, for a heterogeneous medium with scale-dependent parameters which, providing a strong heterogeneity, does not allow to obtain any standard homogeneous medium in the limit.

Topics addressed in the Dissertation. The DISSERTATION provides an introduction to some selected author's papers appended as full texts. Moreover, some extending topics were included in the *introductory part*; although not involved in the appended papers, they are closely related from the theoretical point of view (e.g. homogenization of visco-elastic materials and fading memory phenomenon), or they show further applications which are in the author's research focus, like homogenization in optics.

The main issues discussed in the DISSERTATION are the following:

- **Homogenization applied in wave propagation problems**. Only solid composite materials are considered here (an extension for fluid saturated media has been addressed by the author and will be reported in a forthcoming paper). The main

focus is in the phononic materials ("band-gap materials"), characterized by large heterogeneity in the elasticity coefficients, and in the acoustic transmission on perforated interfaces immersed in the acoustic fluid. Extensions to electromagnetic waves and piezoelectric composites are discussed also. Since all these topics are concerned with material engineering, the issue of optimal design and sensitivity analysis with respect to microstructural parameters is addressed.

- **Homogenization of fluid-saturated porous materials** (FSPM) with *double porosity.* It is shown how different topologies of the microstructure with respect to double porosity lead to qualitatively different models. An extension for large-deforming media was proposed, which is based on linearized subproblems. Finally, homogenization of the *fluid perfusion in layered double-porous medium* is described. These topics have applications in modeling the tissue perfusion and in modeling bone poroelasticity.

1.1 Periodic unfolding and homogenization

The *periodic unfolding method* [CDG08] used in homogenization is an alternative to other homogenization techniques based on asymptotic analysis (see [CD99] and references therein), like classical asymptotic expansion methods, cf. [SP80], or two-scale convergence [All92]. The "unfolding method" (UFM) is employed in the prevailing part of papers included in the DISSERTATION . This method is relatively easy to use for linear, or quasi-linear problems and is very close to the two-scale convergence. Unlike the latter method, the UFM uses through the standard convergence of "unfolded" functions (sequences) defined in the Cartesian product of the macroscopic domain Ω and the *representative periodic cell Y* characterizing the microstructure.

To explain the idea, we consider domain $\Omega \subset \mathbb{R}^3$ being generated as a periodic lattice by the representative cell. Let $Y = \Pi_{i=1,2,3}]0, \bar{y}_i[$ and assume that $\Omega \subset \mathbb{R}^3$ can be covered by copies of εY, i.e. there is a set of integer multi-indices $\mathbb{K}_\Omega \in \mathbb{Z}^3$ so that:

$$\Omega = inter \bigcup_{\boldsymbol{k} \in \mathbb{K}_\Omega} \overline{Y^\varepsilon}(\xi) \quad \text{with } Y^\varepsilon(\xi) = \xi + \varepsilon Y , \quad \xi_i = \varepsilon k_i \bar{y}_i \text{ (no summation)} , \tag{1}$$

where $\overline{Y}$ is the closure of Y and $\varepsilon_0 \geq \varepsilon > 0$. This restriction of the shape of Ω is artificial to simplify the framework and it is not needed in general. Domain Y represents one period of a perfectly periodic "microstructure" constituting the medium.

The coordinates of the position can be split into the "coarse" and "fine" parts. For a given finite $\varepsilon > 0$,

$$x \equiv \varepsilon \left[\frac{x}{\varepsilon}\right]_Y + \varepsilon \left\{\frac{x}{\varepsilon}\right\}_Y = \xi + \varepsilon y , \quad \text{where } y = \left\{\frac{x}{\varepsilon}\right\}_Y \in Y \quad \text{and } \xi = \varepsilon \left[\frac{x}{\varepsilon}\right]_Y , \tag{2}$$

where ξ is given according to (1); such a decomposition is unique, once Y is defined (see Fig. 1). Note that the Gauss bracket $[z_i]_Y$, $i = 1, 2, 3$ is the whole part of $z_i/\bar{y}_i$ and $\{z_i\}_Y$ is the reminder.
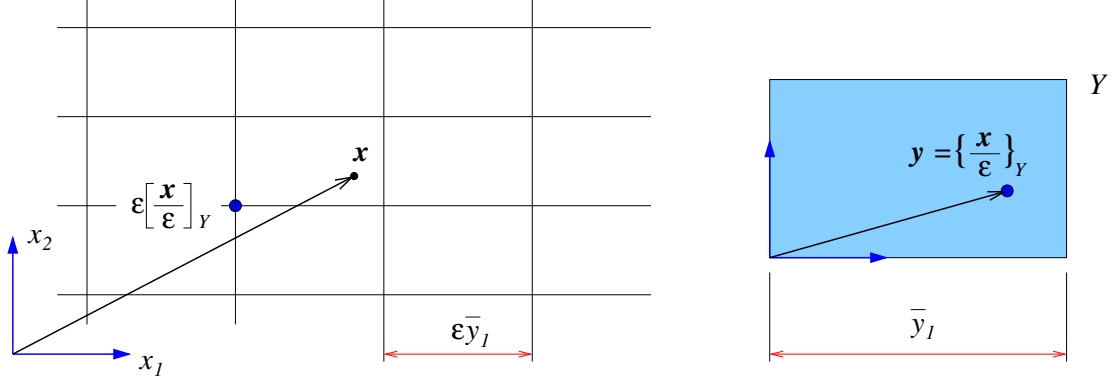
3

Figure 1: Lattice periodic structure of body Ω. Coordinate split into the coarse and the fine parts.

By virtue of the coordinate decomposition (2), any function ψ of x can be unfolded into a function of x and y; in a simplified case, the *unfolding operator* $\mathcal{T}_\varepsilon(\textbf{.})$ can be defined by the following relation:

$$\mathcal{T}_\varepsilon(\psi(x)) = \tilde{\psi}(\xi(x), y(x)) = \psi(\xi(x) + \varepsilon y),$$

where $\xi(x)$ and $y(x)$ are introduced according to (2). For all functions ψ and ϕ, the three following properties are crucial:

$$
\begin{aligned}
i) \quad & \mathcal{T}_\varepsilon(\psi(x)\phi(x)) = \mathcal{T}_\varepsilon(\psi(x))\mathcal{T}_\varepsilon(\phi(x)) , \\
ii) \quad & \int_\Omega \psi(x)\, dx = \int_\Omega \frac{1}{|Y|} \int_Y \mathcal{T}_\varepsilon(\psi)(x, y)\, dx\, dy , \\
iii) \quad & \mathcal{T}_\varepsilon(\nabla_x \psi(x)) = \frac{1}{\varepsilon} \nabla_y \left(\mathcal{T}_\varepsilon(\psi)(x, y) \right) ,
\end{aligned}
\tag{3}
$$

where ∇_x and ∇_y are the gradient operators with respect to x and y respectively. Due the integral transformation $(3)_2$, the standard notion of *weak convergence* in a suitable functional space $W(\Omega, Y)$ can be used (typically $W(\Omega, Y) = L^2(\Omega \times Y)$).

In homogenization, the key issue is convergence of differential operators, like gradients. We can illustrate two situations which occur in problems related to strongly heterogeneous media. Let $W_\#(Y)$ be a space of Y-periodic functions, and consider a *recovery sequence* $\{u^{R\varepsilon}\}, \varepsilon \to 0$ bounded in space $W(\Omega)$, where $u^{R\varepsilon} = u^{0\varepsilon} + \varepsilon u^{1\varepsilon}$ and its gradient are unfolded, as follows:

$$
\begin{aligned}
\mathcal{T}_\varepsilon\left(u^{R\varepsilon}\right) &= u^{0\varepsilon}(\xi + \varepsilon y,\, y) + \varepsilon u^{1\varepsilon}(\xi + \varepsilon y,\, y) , \\
\mathcal{T}_\varepsilon\left(\nabla u^{R\varepsilon}\right) &= \nabla_x u^{0\varepsilon}(x, y) + \frac{1}{\varepsilon} \nabla_y u^{0\varepsilon}(x, y) + \varepsilon \nabla_x u^{1\varepsilon}(x, y) + \nabla_y u^{1\varepsilon}(x, y) ,
\end{aligned}
\tag{4}
$$

where $u^{0\varepsilon}(x, \cdot)$ and $u^{1\varepsilon}(x, \cdot) \in W_\#(Y)$. Further assume the following weak convergences: $u^{0\varepsilon} \rightharpoonup \bar{u}^0$, $\mathcal{T}_\varepsilon(u^{0\varepsilon}) \rightharpoonup u^0$, $\mathcal{T}_\varepsilon(u^{1\varepsilon}) \rightharpoonup u^1$, where u^0, u^1 are two-scale functions in $(x, y) \in \Omega \times Y$ and $\bar{u}^0$ is the mean value of $u^0(x, y)$ given by $|Y|^{-1} \int_Y u^0(x, y)dy$.

4

For all suitable given test functions $\psi(x, y)$, we consider two particular situations of convergence of gradient

1. *Case of minor fluctuations* – gradient correction:

$$\int_\Omega \nabla u^{R\varepsilon}(x)\psi(x, \frac{x}{\varepsilon}) = \fint_{\Omega \times Y} \mathcal{T}_\varepsilon(\nabla u^{R\varepsilon})(x, y)\,\psi(x, y) \to \fint_{\Omega \times Y} (\nabla_x u^0 + \nabla_y u^1)\psi \;,$$

   where $\nabla_y u^0 = 0$, i.e. $u^0(x, y) \equiv \bar{u}^0(x)$. Thus, u^0 presents the macroscopic part, being independent of the microscopic variables.

2. *Case of strong micro-macro interactions*:

$$\varepsilon \int_\Omega \nabla u^{R\varepsilon}(x)\psi(x, \frac{x}{\varepsilon}) = \varepsilon \fint_{\Omega \times Y} \mathcal{T}_\varepsilon(\nabla u^{R\varepsilon})(x, y)\,\psi(x, y) \to \fint_{\Omega \times Y} \nabla_y u^0(x, y)\psi(x, y) \;,$$

   whereby $u^1 = 0$, *i.e.* the "classical" fluctuations u^1 are of a lower magnitude which are not captured by the first-order homogenization.

The first case is commonly used for standard composites with scale-independent coefficients The second case is characteristic for media with coefficients diminishing with decreasing size of the microstructure; for example, such a model can approximate deformations of very soft elastic material. Combination of the two cases arises in modeling *large contrast composites*, therefore, it is of great importance for this DISSERTATION .

Literature used , related to Section 1 (selection): [All89] [All92] [Ben78] [Bra02] [CD99] [CDG08] [CDGO08] [CSJP99] [MT07] [NNH] [OSY92] [SV04] [Zv02]

2 Wave propagation and dispersion in heterogeneous media

In the context of the homogenization method, waves in solid composites and solid-fluid mixtures have been discussed e.g. in [SP80]. The classical treatment of elastic waves leads to vanishing wave dispersion in the limit $\varepsilon \to 0$, however, the approach reported in the DISSERTATION allows to retain the dispersion properties even in the limit; this is possible due to the *strong heterogeneity* – large contrast in the elasticity coefficients and the special scaling ansatz of these coefficients. Besides the elastic composites, the DISSERTATION addresses also some other topics related to wave propagation, namely the following ones were considered:

1. piezo-materials, i.e. homogenization of piezoelectric composites,

2. phononic materials, i.e. homogenization of vibrating elastic composites with large contrasts in elasticity of the components, which confines propagation of waves for certain polarizations and frequency bands,

3. acoustic waves on a perforated interface, i.e. homogenization of the acoustic transmission conditions taking into account the geometry of periodic perforations,

4. wave propagation of electromagnetic waves in heterogeneous media.

Combinations of all these topics are natural in the view of modeling smart systems transmitting waves:

- *Piezo-phononic materials* form a quite natural extension of the purely elastic phononic materials, they provide even more flexibility in designing smart devices, due to possible interplay between the electric field and deformations. The homogenization issues were discussed in [22, 23, 3].

- There is a natural application of the above mentioned 3rd topic in vibro-acoustics. It is desirable to extend the acoustic transmission conditions for *compliant perforated plates*, when the plate elasticity cannot be neglected. Moreover, the surface acoustic waves propagating along the interface may interfere with the plate structure – the plate can be constructed as a phononic, or piezo-phononic material, so that band gaps of the plate can influence qualitatively the acoustic transmission in the surrounding medium.

- For homogenization of the electromagnetic waves, analogical methods and modeling approaches are applied, as those introduced in the study of elastic waves. Moreover, in combination with piezoelectric materials, coupling between acoustic and electromagnetic waves is a relevant issue.

2.1 Piezo-materials

The piezoelectric effect, coupling deformation and the electric field, is the principle of many smart systems. Apart of vast industrial applications in building electronic devices, piezoelectricity of dry bone indicates a possible usage of this effect in development of new bio-materials. Such idea was considered in [9] where homogenization of elastic anisotropic inclusions populating the piezoelectric matrix was described. The electro-mechanic transduction plays important role in controlling the acoustic wave propagation; in this context, homogenization of piezoelectric (PZ) composite was treated in [22, 3].

Properties of a three dimensional body made of the PZ material are described by three tensors: the elasticity tensor c_{ijkl}^{ε}, the dielectric tensor d_{ij} and the piezoelectric coupling tensor g_{kij}^{ε}, where $i, j, k = 1, 2, \ldots, 3$. The following symmetries hold: $c_{ijkl}^{\varepsilon} = c_{jikl}^{\varepsilon} = c_{klij}^{\varepsilon}$, $d_{ij}^{\varepsilon} = d_{ji}^{\varepsilon}$ and $g_{kij}^{\varepsilon} = g_{kji}^{\varepsilon}$. The state of the PZ material is described by the displacement field $\boldsymbol{u}^{\varepsilon}$ and the voltage (electric potential) φ^{ε}. The PZ coupling is represented by coefficients g_{kij}^{ε} involved in the constitutive relations for the stress, $\boldsymbol{\sigma}^{\varepsilon} = (\sigma_{ij}^{\varepsilon})$ and the electric displacement $\boldsymbol{D}^{\varepsilon} = (D_k^{\varepsilon})$

$$
\begin{aligned}
\sigma_{ij}^{\varepsilon} &= c_{ijkl}^{\varepsilon} e_{kl}(\boldsymbol{u}^{\varepsilon}) - g_{kij}^{\varepsilon} \partial_k \varphi^{\varepsilon}, \\
D_k^{\varepsilon} &= g_{kij}^{\varepsilon} e_{kl}(\boldsymbol{u}^{\varepsilon}) + d_{kl}^{\varepsilon} \partial_l \varphi^{\varepsilon}.
\end{aligned}
\tag{5}
$$

6

The local static equilibrium of the PZ material is expressed by the differential equations

$$\operatorname{div}\boldsymbol{\sigma}^\varepsilon = \boldsymbol{f}^\varepsilon, \qquad \operatorname{div}\boldsymbol{D}^\varepsilon = q^\varepsilon, \tag{6}$$

where $\boldsymbol{f}^\varepsilon$ and q^ε are the volume force and charge, respectively.

Homogenization of a standard PZ heterogeneous medium leads to the effective constitutive law of the form (5) whereby the effective material parameters are computed for a specific microstructure. In [21] we show that combination of two standard PZ materials can give rise a new material with unusual and interesting properties (new non-zero entry in the coupling tensor) — this is the key for designing the so-called metamaterials, *cf.* [23, 7], and the homogenization method serves as an efficient computational tool.

The PZ materials with large contrasts (respected by scaling in analogy with (8)) in all coefficients involved in (5) were considered in homogenization of *phononic materials*, see [22, 3].

2.2   Phononic materials

The *phononic materials (crystals)* are multi-phasic (bi-phasic) elastic media with periodic structure and with large contrasts in elasticity of the phases. Often they are called the *phononic band-gap materials* due to their essential property to suppress propagation of elastic waves in certain frequency ranges. The phononic crystals are used in modern technologies to generate frequency filters, beam splitters, sound or vibration protection devices (for noise reduction), or they may serve as waveguides. Similar phenomena in the propagation of the electromagnetic field were studied even before in the context of the *photonic crystals*.

The method of homogenization provides a useful modeling tool which allows for prediction of the band gap distribution for stationary or long guided waves. The "standard computational approach" based on a full heterogeneous model requires to evaluate the whole Brillouin zone for the dispersion diagram reconstruction; as the consequence, it leads to a killing computational complexity. On the other hand, the homogenized model captures the essential features of the phononic material and may serve a good approximation of the band-gap prediction, while keeping the computational complexity at a very low level. As an advantage, the homogenized model can be employed in inverse problems like optimal design of phononic structures.

2.2.1   Periodic strongly heterogeneous material

We consider an open bounded domain $\Omega \subset \mathbb{R}^3$ and the reference (unit) cell $Y =]0,1[^3$ with an embedded inclusion $\overline{Y_2} \subset Y$, whereby the matrix part is $Y_1 = Y \setminus \overline{Y_2}$. Let us note, that Y may be defined more generally as a parallelepiped. Using the reference cell we generate the decomposition of Ω into the union of inclusions and the matrix. Inclusions have the size $\sim \varepsilon$,

$$\Omega_2^\varepsilon = inter \bigcup_{k \in \mathbb{K}^\varepsilon} \varepsilon(\overline{Y_2} + k)\,, \text{ where } \mathbb{K}^\varepsilon = \{k \in \mathbb{Z}|\ \varepsilon(k + \overline{Y_2}) \subset \Omega\}\,, \tag{7}$$

whereas the perforated matrix is $\Omega_1^\varepsilon = \Omega \setminus \overline{\Omega_2^\varepsilon}$.

We assume that inclusions are occupied by a "very soft material" in the sense that the coefficients of *the elasticity tensor in the inclusions* are significantly smaller than those of the matrix compartment, however *the material density* is comparable in both the compartments. Such structures exhibit remarkable band gaps; this was proved by both experiments and modeling. Here, as an important feature of the modeling based on asymptotic analysis, the ε^2 scaling of elasticity coefficients in the inclusions appears; the following ansatz is considered:

$$\rho^\varepsilon(x) = \left\{ \begin{array}{ll} \rho^1 & \text{in } \Omega_1^\varepsilon, \\ \rho^2 & \text{in } \Omega_2^\varepsilon, \end{array} \right. \qquad c_{ijkl}^\varepsilon(x) = \left\{ \begin{array}{ll} c_{ijkl}^1 & \text{in } \Omega_1^\varepsilon, \\ \varepsilon^2 c_{ijkl}^2 & \text{in } \Omega_2^\varepsilon. \end{array} \right. \tag{8}$$

In analogy, the PZ phononic materials can be treated.

2.2.2   Modeling the stationary waves

We consider stationary wave propagation in the medium introduced above. Although the problem can be treated for a general case of boundary conditions, for simplicity we restrict the model to the description of clamped structures loaded by volume forces. We assume harmonic single-frequency volume forces $\boldsymbol{F}(x,t) = \boldsymbol{f}(x)e^{i\omega t}$, where $\boldsymbol{f} = (f_i), i = 1, 2, 3$ is its local amplitude and ω is the frequency. Correspondingly, a dispersive displacement field with the local magnitude $\boldsymbol{u}^\varepsilon$ has the form $\boldsymbol{U}^\varepsilon(x, \omega, t) = \boldsymbol{u}^\varepsilon(x, \omega)e^{i\omega t}$. This allows us to study the steady periodic response of the medium, as characterized by displacement field $\boldsymbol{u}^\varepsilon$ which satisfies the following boundary value problem:

$$\begin{aligned} -\omega^2 \rho^\varepsilon \boldsymbol{u}^\varepsilon - \text{div}\,\boldsymbol{\sigma}^\varepsilon &= \rho^\varepsilon \boldsymbol{f} \quad \text{in } \Omega, \\ \boldsymbol{u}^\varepsilon &= 0 \quad \text{on } \partial\Omega, \end{aligned} \tag{9}$$

where the stress tensor $\boldsymbol{\sigma}^\varepsilon = (\sigma_{ij}^\varepsilon)$ is expressed in terms of the linearized strain tensor $\boldsymbol{e}^\varepsilon = (e_{ij}^\varepsilon)$ by the Hooke's law $\sigma_{ij}^\varepsilon = c_{ijkl}^\varepsilon e_{kl}(\boldsymbol{u}^\varepsilon)$.

2.2.3   Homogenized model

Due to the *strong heterogeneity* in the elastic coefficients, the homogenized model exhibits dispersive behaviour; this phenomenon cannot be observed when standard two-scale homogenization procedure is applied to a medium without scale-dependent material parameters. In [1] the unfolding operator method of homogenization [CDG08] was applied with the strong heterogeneity ansatz (8) and in [22] the analogous result was obtained for the piezoelectric material with the strong heterogeneity scaling.

The resulting limit equations, as derived in [1], describe the structure behaviour at the "macroscopic" scale. They involve the homogenized coefficients which depend on the characteristic responses at the "microscopic" scale.

The frequency–dependent homogenized mass involved in the macroscopic momentum equation is expressed in terms of eigenelements $(\lambda^r, \boldsymbol{\varphi}^r) \in \mathbb{R} \times \mathbf{H}_0^1(Y_2)$, $r = 1, 2, \ldots$ of the elastic spectral problem which is imposed in inclusion Y_2 with $\boldsymbol{\varphi}^r = 0$ on ∂Y_2:

$$\int_{Y_2} c_{ijkl}^2 e_{kl}^y(\boldsymbol{\varphi}^r) e_{ij}^y(\boldsymbol{v}) = \lambda^r \int_{Y_2} \rho^2 \boldsymbol{\varphi}^r \cdot \boldsymbol{v} \quad \forall \boldsymbol{v} \in \mathbf{H}_0^1(Y_2) , \quad \int_{Y_2} \rho^2 \boldsymbol{\varphi}^r \cdot \boldsymbol{\varphi}^s = \delta_{rs} . \tag{10}$$

To simplify the notation we introduce the *eigenmomentum* $\boldsymbol{m}^r = (m_i^r)$,

$$\boldsymbol{m}^r = \int_{Y_2} \rho^2 \boldsymbol{\varphi}^r. \tag{11}$$

The effective mass of the homogenized medium is represented by mass tensor $\boldsymbol{M}^* = (M_{ij}^*)$, which is evaluated as

$$M_{ij}^*(\omega^2) = \frac{1}{|Y|} \int_Y \rho \delta_{ij} - \frac{1}{|Y|} \sum_{r \geq 1} \frac{\omega^2}{\omega^2 - \lambda^r} m_i^r m_j^r ; \tag{12}$$

The elasticity coefficients are computed just using the same formula as for the perforated matrix domain, thus being independent of the material in inclusions:

$$C_{ijkl}^* = \frac{1}{|Y|} \int_{Y_1} c_{pqrs} e_{rs}^y(\boldsymbol{w}^{kl} + \boldsymbol{\Pi}^{kl}) e_{pq}(\boldsymbol{w}^{ij} + \boldsymbol{\Pi}^{ij}) , \tag{13}$$

where $\boldsymbol{\Pi}^{kl} = (\Pi_i^{kl}) = (y_l \delta_{ik})$ and $\boldsymbol{w}^{kl} \in \mathbf{H}_\#^1(Y_1)$ are the corrector functions satisfying

$$\int_{Y_1} c_{pqrs} e_{rs}^y(\boldsymbol{w}^{kl} + \boldsymbol{\Pi}^{kl}) e_{pq}^y(\boldsymbol{v}) = 0 \quad \forall \boldsymbol{v} \in \mathbf{H}_\#^1(Y_1) . \tag{14}$$

Above $\mathbf{H}_\#^1(Y_1)$ is the restriction of $\mathbf{H}^1(Y_1)$ to the Y-periodic functions (periodicity w.r.t. the homologous points on the opposit edges of ∂Y).

The *homogenized equation* of the "macromodel", here presented in its differential form, describes the macroscopic displacement field $\boldsymbol{u}$:

$$\omega^2 M_{ij}^*(\omega) u_j + \frac{\partial}{\partial x_j} C_{ijkl}^* e_{kl}(\boldsymbol{u}) = M_{ij}^*(\omega) f_j , \tag{15}$$

where M_{ij}^* at the r.h.s. loading term appears due to the volume forces in (9) proportional to the density.

Using this equation, the dispersion of guided waves can be studied, see [24]. Heterogeneous structures with finite scale of heterogeneities exhibit the frequency *band gaps* for certain frequency bands. In the *homogeneized medium*, waves can be propagated provided the mass tensor $\boldsymbol{M}^*(\omega)$ is positive definite, or positive semidefinite; this effect is explained below.

We can derive a homogenized model analogous to (15) also for the *piezoelectric phononic* (piezo-phononic) materials with "soft inclusions", i.e. the scaling (8) is adopted also for parameters d_{ij} and g_{kij}, see (5). In this case, however, the spectral problem analogous to (10) comprises an additional constraint arising from electric charge conservation, see [22, 3] for details.

2.2.4 Band gap prediction

As the main advantage of the homogenized model (15), by analyzing the dependence $\omega \to \boldsymbol{M}^*(\omega)$ one can determine distribution of the band gaps; it was proved in [1], *cf.* [24] that there exist frequency intervals G^k, $k = 1, 2, \dots$ such that for $\omega \in G^k \subset]\lambda^k, \lambda^{k+1}[$ at least one eigenvalue of tensor $M_{ij}^*(\omega)$ is negative. Those intervals where all eigenvalues γ_M of M_{ij}^* are negative are called *strong*, or *full* band gaps. In the latter case the negative sign of the mass changes the hyperbolic type of the wave equation to the elliptic one, therefore, no waves can propagate. In the "weak" bad gap situation only waves with certain polarization can propagate, as explained below.

The band gaps can be classified w.r.t. the waves polarization which is determined in terms of the eigenvectors of $M_{ij}^*(\omega)$. Given a frequency ω, there are three cases to be distinguished according to the signs of eigenvalues $\gamma_M^r(\omega)$, $r = 1, 2, 3$ (in 3D), determining the "positivity, or negativity" of the mass:

1. **propagation zone** – All eigenvalues of $M_{ij}^*(\omega)$ are positive: then homogenized model (15) admits wave propagation without any restriction of the wave polarization;

2. **strong band gap** – All eigenvalues of $M_{ij}^*(\omega)$ are negative: then homogenized model (15) does *not* admit any wave propagation;

3. **weak band gap** – Tensor $M_{ij}^*(\omega)$ is indefinite, i.e. there is at least one negative and one positive eigenvalue: then propagation is possible only for waves polarized in a manifold determined by eigenvectors associated with positive eigenvalues. In this case the notion of wave propagation has a local character, since the "desired wave polarization" may depend locally on the position in Ω.

In Fig. 2 we introduce a graphical illustration of the band gaps analyzed for an L-shaped inclusions. If inclusions (considered in 2D) are symmetric w.r.t. more than 1 axis of symmetry, than only strong band gaps exist. More details on the band gap properties and their relationship to the dispersion of guided waves were discussed in [24]. For piezo-phononic materials the above mentioned statements on the structural symmetry do not hold in general because of the material anisotropy of piezoelectric materials, thus, typically only the weak band gaps exist [3].

2.3   Acoustic wave transmission on perforated interfaces

Homogenization can be employed to develop approximate models of various transmission and transport phenomena on thin interfaces characterized by a "microstructure" [CDGO08]. In the DISSERTATION , the homogenization is applied to approximate the acoustic transmission between two halfspaces separated by an interface formed as a solid (rigid) plate perforated periodically by holes of arbitrary shapes, so that the two halfspaces are connected. We consider the acoustic medium occupying domain Ω^G which is subdivided by perforated plane Γ_0 in two disjoint subdomains Ω^+ and Ω^-, so that $\Omega^G = \Omega^+ \cup \Omega^- \cup \Gamma_0$. Denoting by p the acoustic pressure field in $\Omega^+ \cup \Omega^-$, in a case of no convection flow, the
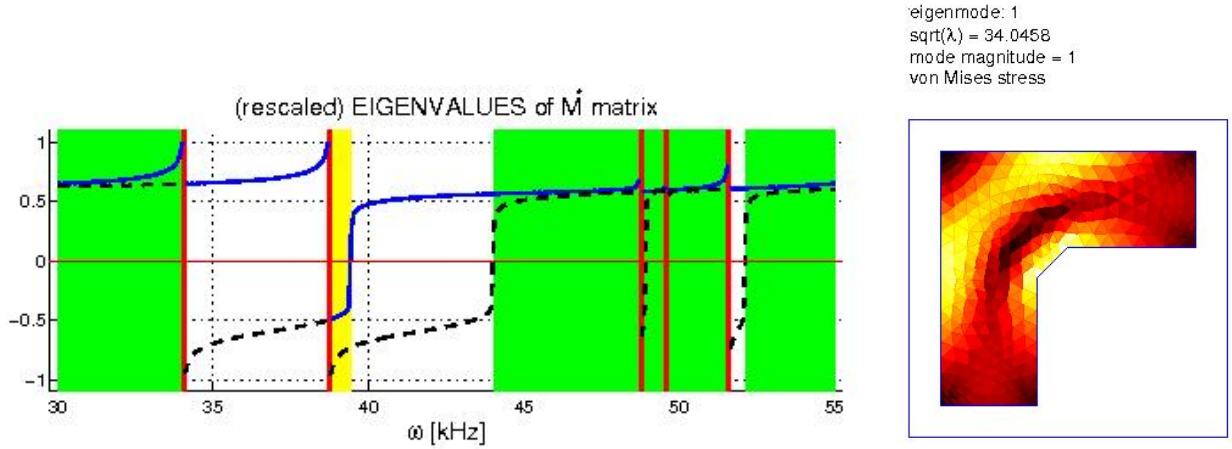
Figure 2: Left: weak band gaps (white) and strong band gaps (yellow) computed for an elastic composite with L-shaped inclusions, the green bands are propagation zones (the solid and dashed curves describe eigenvalues of $\mathbf{M}^*(\omega)$); Right: the first eigenmode of the L-shaped clamped elastic inclusion.

acoustic waves in Ω^G are described by the following equations (ω is the frequency of the incident wave related to wave number k through the speed of sound propagation $c = \omega/k$),

$$c^2 \nabla^2 p + \omega^2 p = 0 \quad \text{in } \Omega^- \cup \Omega^+ \,,$$
$$+ \text{ boundary conditions} \quad \text{on } \partial\Omega^G \,, \tag{16}$$

supplemented by transmission conditions on interface Γ_0. In [20] such conditions were obtained by the two-scale homogenization of a layer with an immersed sieve-like obstacle. In Figure 3 we illustrate such a layer $\Omega_\delta = \Gamma_0 \times] - \delta/2, \delta/2[\subset \mathbb{R}^3$ embedded in $\Omega^G = \Omega_\delta^+ \cup \Omega_\delta^+ \cup \Omega_\delta \cup \Gamma_\delta^\pm$. The acoustic medium occupies domain $\Omega_\delta^\varepsilon = \Omega_\delta \setminus \overline{S_\delta^\varepsilon}$, where S_δ^ε is the solid *rigid* obstacle which in a simple layout has a form of the periodically perforated slab. However, the aim of the study [20] was to obtain transmission conditions which describe quite general shape of periodic perforations.

To derive the transmission conditions, the acoustic waves in the layer were subject to asymptotic analysis w.r.t. size of the perforation ε which is related to the thickness $\delta = h\varepsilon$, where $h > 0$ is fixed. The acoustic potential $p^{\varepsilon\delta}$ satisfies the Helmholtz equation in $\Omega_\delta^\varepsilon$

$$c^2 \nabla^2 p^{\varepsilon\delta} + \omega^2 p^{\varepsilon\delta} = 0 \quad \text{in } \Omega_\delta^\varepsilon \,,$$
$$c^2 \frac{\partial p^{\varepsilon\delta}}{\partial n^\delta} = -\mathrm{i}\omega g^{\varepsilon\delta\pm} \quad \text{on } \Gamma_\delta^\pm \,, \tag{17}$$
$$\frac{\partial p^{\varepsilon\delta}}{\partial n^\delta} = 0 \quad \text{on } \partial S_\delta^\varepsilon \cup \partial\Omega_\delta^\infty \,,$$

where by n^δ we denote the normal vector outward to Ω_δ. Assuming convergence of the interface fluxes (velocities) $g^{\varepsilon\delta} \to g^0$ (in a sence), by homogenization $\varepsilon \to 0$, convergence of
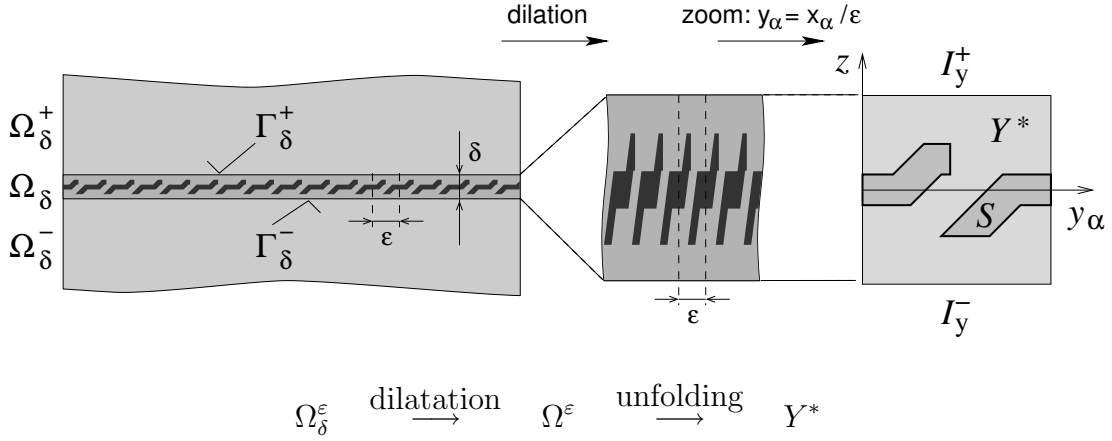
11

dilation → zoom: $y_\alpha = x_\alpha / \varepsilon$ →

$$\Omega_\delta^\varepsilon \xrightarrow{\text{dilatation}} \Omega^\varepsilon \xrightarrow{\text{unfolding}} Y^*$$

Figure 3: Left: global problem imposed in entire domain Ω^G before homogenization of the layer Ω_δ. Right: representative cell of the periodic structure. The dark patterns represent the obstacles in the fluid.

$p^{\varepsilon\delta} \to p^0$ is obtained and (17) tranforms into the following equations involving homogenized coefficients A, B, F and the layer porosity f^*,

$$-\partial_\alpha(A_{\alpha\beta}\partial_\beta p^0) + \omega^2 f^* p^0 - \mathrm{i}\omega\partial_\alpha(B_\alpha g^0) = 0 \quad \text{on } \Gamma_0 \ ,$$

$$-\mathrm{i}\omega h B_\beta \partial_\beta p^0 + \omega^2 F g^0 = -\mathrm{i}\omega\frac{1}{\varepsilon_0}[p]_-^+ \quad \text{on } \Gamma_0 \ , \tag{18}$$

$$A_{\alpha\beta}\partial_\beta p^0 = 0 \quad \text{on } \partial\Gamma_0 \ ,$$

where $[p]_-^+/\varepsilon_0$ is the jump of p relative to the "real" layer thickness $h\varepsilon_0 > 0$ and is evaluated on Γ_0 by the acoustic potential field p in Ω^G. To compute A, B, F, microscopic problems have to be solved in the reference microscopic cell $Y^* = Y \setminus \overline{S}$, where domain S represents the obstacle generating the perforation, see Fig. 3 (right).
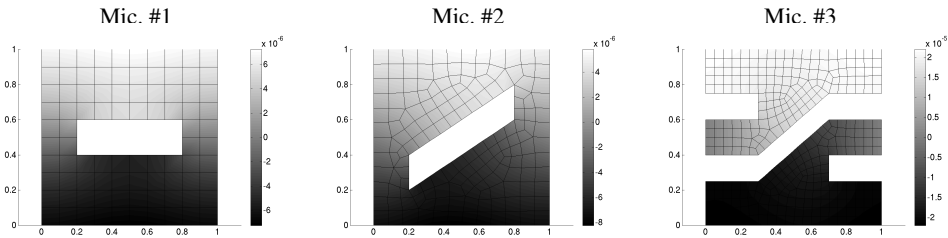

Figure 4: Microscopic response in Y^* for different types of microstructures in 2D. $B = 0$ only for Mic. #1, while $B = -0.251m$ for Mic. #2 and $B = -0.897m$ for Mic. #3

For the "global problem" (16), the transmission conditions are presented in an implicit form by equations (18): they couple $[p]_-^+$ with normal derivatives $\partial p/\partial n^+ = -\partial p/\partial n^- = -\mathrm{i}\omega g^0$, whereby p^0 describing the "in-layer" wave serves as an internal variable of the model. Out of resonances, p^0 vanishes when $(B_\beta) = 0$, see Fig. 4
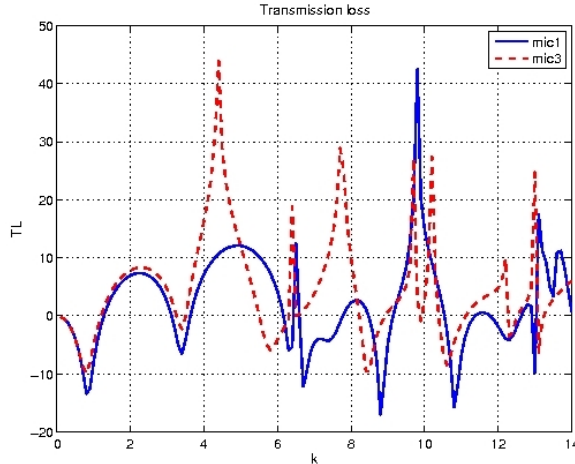
12

Figure 5: Transmission losses for two perforation types: solid (mic1) microstructure #1, dashed (mic3) microstructure #3, see Fig. 4. (Computed by V. Lukeš, December 2010)

To illustrate influence of the perforation design on the global acoustic response in domain Ω^G, in Fig. 5 the transmission losses for a waveguide fitted with two different perforations on Γ_0 is depicted.

2.4 On metamaterials and the design sensitivity analysis

By 'metamaterials' we refer to materials which exhibit 'non-conventional material properties'. Those materials typically are not found in nature. Metamaterials are most often man-made (artificial), being engineered using modern technologies for a wide range of applications. The principle of designing such materials is based on the multiscale approach: by terminology used in this thesis, on composing different traditional materials attaining a suitable structural arrangement at the "microscopic level", we can modify the properties observed at the "macroscopic level". Thus, the apparent behaviour may depend on the "microstructural" (nano-structural) interactions associated with a characteristic length. Among the well-known examples we can mention the negative Poisson ratio materials in elasticity, or the so-called left-handed materials in nano-optics. Moreover, due to multi-physical interactions relevant at the smaller scale, the "macroscopic" material properties associated with one field can be modified by other fields relevant at the "microscopic" level where the interactions are non-negligible.

Metamaterial properties, therefore, emerge under the controlled influence of microstructures. Inclusions at the "microscopic" level described by their material properties and their shape are to be designed in order to approach certain desired material properties.

As an example of metamaterial optimization, we can design a phononic material described in Section 2.2.3 so that the lowest band-gaps are maximized. In [23] the non-smooth sensitivity of the band gap bounds were developed, admitting also multiple eigen-modes involved in the expansion of the mass tensor. In Fig. 6 an example of band gap maximiza-

13

tion is illustrate using the "initial" and "optimized" band-gap diagrams and corresponding reference cells. The design parameters described the inclusion shape.
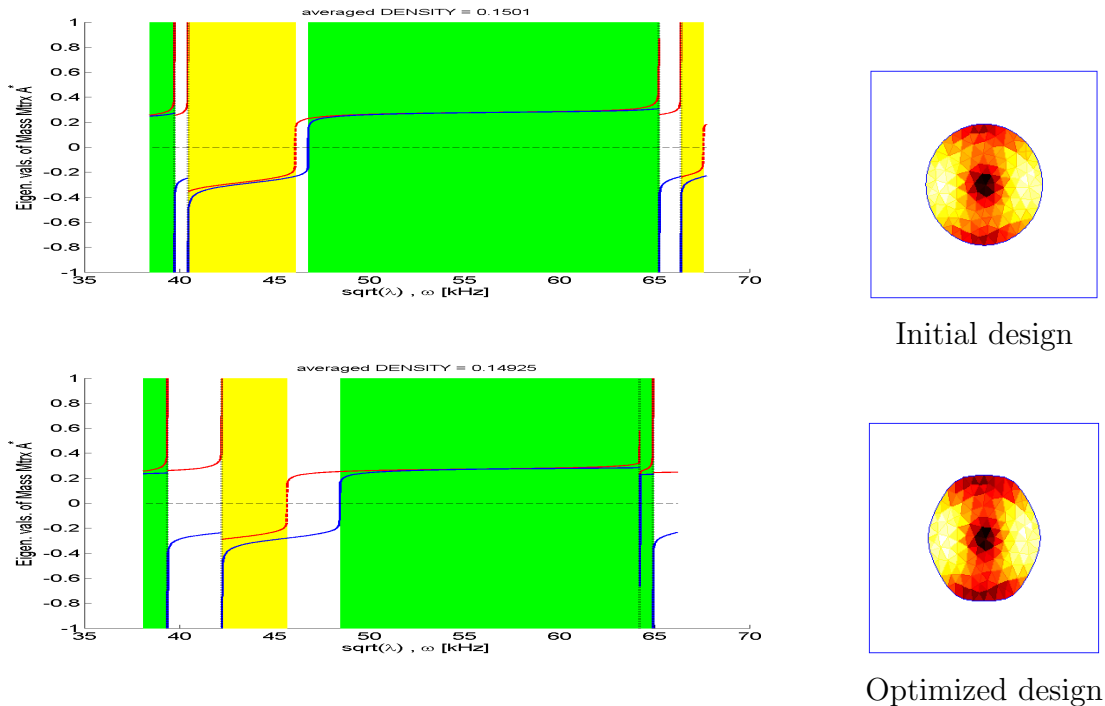

Initial design

Optimized design

Figure 6: Left: band gap distribution in the initial and optimized structures; yellow – strong gaps, white – weak gaps. Right: corresponding shapes of inclusion Y_2 with illustrated von Mises stress associated with the 2nd eigenmode, (λ^2, φ^2), see Sections 2.2.3 and 2.2.4.

Literature used , related to Section 2 (selection): [AK04] [BF04] [BCZ87] [BD94] [HCK86] [HM03] [HN88] [MW07] [RD00] [SJ03] [JP06] [SP80]

3 Fluid saturated porous media (FSPM) with dual porosity

The models of *fluid saturated porous media* (FSPM) which we have in mind are relevant to the scale where individual fluid-filled pores are not distinguishable, so that at any point of the bulk material both the solid and fluid phases are present, being distributed according to the volume fractions, cf. [Cou04, dB00]. The phenomenological description was developed by M. Biot [Bio55]; his model is considered here as a basis for modeling media with large contrasts in the hydraulic permeability coefficients, thus, presenting the *strong heterogeneity*. Such a modeling option is related to the notion of the double porosity

[AB92, ADH90] which introduces yet another scale with even smaller characteristic size than the one characterizing the "microscopic level".

In the DISSERTATION two important and *general phenomena* are demonstrated when homogenizing the FSPM:

- In high contrast media, in general, the topology of the microstructure decomposition influences qualitatively the homogenization result. We consider the Biot continuum where the strong heterogeneity (in the permeability coefficients) is introduced for two different topologies of the reference cell decomposition. In the limit $\varepsilon \to 0$, two qualitatively different models are obtained.

- When evolutionary models are homogenized, the fading memory effect features the resulting limit model. In the context of the FSPM, the memory effects of the homogenized constitutive laws arise from the fluid microflow governed by the Darcy law.

3.1 Biot model and double porosity

The Biot model involves three essential constitutive laws: 1) the relationship between the drained solid skeleton "macroscopic" deformation $\boldsymbol{e}(t,x)$, the fluid pressure in pores $p(t,x)$ and the total stress $\boldsymbol{\sigma}(t,x)$, 2) the relationship between the variation of the fluid content, skeleton (macroscopic) deformation, and the fluid pressure, 3) the Darcy law relating the seepage velocity, $\boldsymbol{w}(t,x)$, with "dynamic fluid pressure", i.e. the static part $p(t,x)$ and the fluid inertia part. In the DISSERTATION , only quasistatic problems are studied so that the following form of the equations is relevant:

$$
\begin{aligned}
-\nabla \cdot (\boldsymbol{I\!D}\,\boldsymbol{e}(\boldsymbol{u})) + \nabla \cdot (\boldsymbol{\alpha} p) &= \boldsymbol{f} \; , \\
\boldsymbol{K}^{-1}\boldsymbol{w} + \nabla p &= 0 \; , \\
\boldsymbol{\alpha} : \boldsymbol{e}(\dot{\boldsymbol{u}}) + \nabla \cdot \boldsymbol{w} + \frac{1}{\mu}\dot{p} &= 0 \; ,
\end{aligned}
\tag{19}
$$

where $\boldsymbol{I\!D}$ is the elasticity tensor associated to the drained skeleton, $\boldsymbol{K}$ is the hydraulic permeability (specific to a given fluid), α is the poroelastic stress coefficient and μ is the Biot modulus which depends on compressibility of the solid skeleton and fluid. Obviously, the three field formulation can be reduced to the two field formulation by eliminating $\boldsymbol{w}$, so that (19) becomes

$$
\begin{aligned}
-\nabla \cdot (\boldsymbol{I\!D}\,\boldsymbol{e}(\boldsymbol{u})) + \nabla \cdot (\boldsymbol{\alpha} p) &= \boldsymbol{f} \; , \\
\boldsymbol{\alpha} : \boldsymbol{e}(\dot{\boldsymbol{u}}) - \nabla \cdot \boldsymbol{K}\nabla p + \frac{1}{\mu}\dot{p} &= 0 \; .
\end{aligned}
\tag{20}
$$

Further reduction of the model is possible when both the phases are incompressible, i.e. when $1/\mu \to 0$ and $\boldsymbol{\alpha} \to \boldsymbol{I}$.

3.1.1 Double porosity and permeability scaling

The *dual porosity* denotes a "second" porosity in the "dual-porous" medium; it means that the two porosities are qualitatively different. In our setting, the *primary* porosity is featured by pores which are substantially larger than those of the "dual" porosity. In the context of microstructures, the two porosities are associated with different levels of the structure, i.e. with different characteristic lengths.
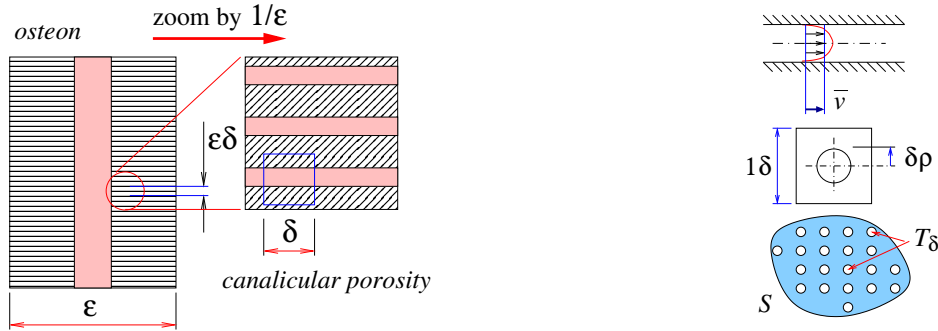

Figure 7: Left: schematic illustration of the osteon double porous structure. Right: a scheme explaining the permeability δ^2-dependence due to the velocity profile in an array of canals. The total perfused area S is perforated by canals with total cross-section T_δ (bottom), each canal has the cross-section $\pi\rho^2\delta^2$; the square periodic cell is shown (middle) as well as the velocity profile in one canal. (top).

Although the notion of the double porosity and of the double porous media are standard and generally accepted, see [Hor97] and the references cited therein, for the sake of completeness, we shall give the reasons which justify modeling of the flow in the *dual porosity* using the Darcy law with the *high contrast permeability*. In the context of the homogenization procedure, the permeability coefficients depend on the characteristic scale of the representative volume.

The double porous media are frequent in nature. Besides various fissured rocks, the dual porosity is presented by the canalicular network of the so-called matrix constituting the structure of cortical bone tissue, see Fig. 8, [25].

In the *dual porosity*, the permeability coefficient is proportional to ε^2, where ε is the dimensionless scale parameter. In Fig. 7, the *dual porosity* is represented by an array of"horizontal" channels of the canalicular porosity. The mean velocity in each channel is proportional to the pressure gradient, being governed by the Poiseuille flow, whereby the proportionality constant is given by the square of the radius, i.e. by δ^2. The ratio between the macro-, meso- and micro- scales is the same, i.e. $\delta \sim \varepsilon$, hence the scale dependent permeability $\sim \varepsilon^2$: the seepage in the dual porosity is given $\boldsymbol{w}^\varepsilon = -\varepsilon^2 \boldsymbol{K}_\nu \nabla p$, where $\boldsymbol{K}_\nu$ is disproportional to the fluid viscosity.

3.2 Homogenization of FSPM with application in biomechanics

The theory of FSPM has been developed in adherence to applications in civil engineering, oil industry, mining and rock mechanics. Also the tissue biomechanics presents a new challenging field of applications, due to large complexity of processes and interactions undergoing in living tissues.

In contrast with soils, rocks and materials used in civil engineering, the biological materials exhibit much larger organization of their structure. To illustrate the difference, one can consider seepage and consolidation in moist soils, on one hand, and the sophisticated system of heart muscle perfusion, on the other hand. In both these cases, the material contains the solid and liquid phases, however, the structure of pores is very different.

In the DISSERTATION several models of biological tissues were treated using homogenization with the dual porosity ansatz.

- The *smooth muscle tissue* model [13] is based on the large deforming FSPM with locally periodic structure. The representative cell contains the fluid-filled inclusion representing the muscle cell. The cytoskeleton is approximated very roughly as a truss with prestretch corresponding to the cell contraction. The extracellular space (the matrix) represents the dual porosity, whereby fluid can flow between the matrix and the cell due permeability of the cell surface. Although from the physiological point of view this model is naive, it contains some important features and can serve as a basis for further model improvements and investigations of the mechanical interactions related to various regimes of tissue contraction.

- The *compact bone* poroelasticity model [25, 15] describes interactions between deformation of the bone tissue and induced flow in the double-porous structure consisting of the Havers-Volkmann channels (the primary porosity) and the canaliculi (the dual porosity). This model is being developed to understand how the flow in the canaliculi populated by mechano-sensitive bone cells depends on the macroscopic load, since this phenomenon influences significantly the bone tissue growth and remodeling.

- The model describing *blood perfusion in deforming tissue* [12, 16, 19] is relevant to the lower levels of the "perfusion tree". The two systems of channels characterize the arterial and venous sectors which exchange the fluid (bood) through the matrix representing the dual porosity. The model has been extended for the large deformation using the linearization based on the updated Lagrangian formulation.

- The model of *blood perfusion in "layered tissues"* [14] is an attempt to cope with branching organization of the perfusion tree. The tissue periodicity is confined to two directions associated with the layer mean-surface, whereas there is no periodicity in the transversal direction. Thus, the tissue volume in 3D can be decomposed into several layers and the homogenization provides several 2D coupled problems, one per each layer.
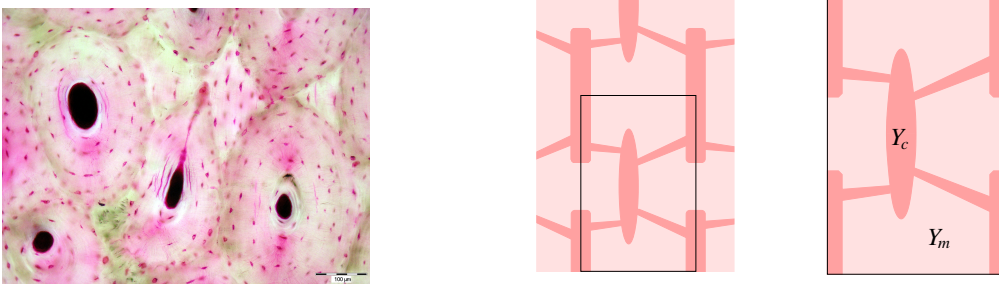
Figure 8: **Left:** a micrograph of the osteon porosity arranged in cylindrical geometry. The Haversian canals form the center of each osteon bounded by the cement line. The osteon matrix is penetrated by canalicular porous network arranged almost radially with respect to the osteon axis. (The color image provided by courtesy of Zbyněk Tonar.) **Right:** microstructure decomposition w.r.t. the dual porosity: dark pink: Ω_c, light pink: Ω_m, and the representative periodic cell Y decomposition.

3.2.1   Two compartment topology of the microstructure

The two compartment topology of the microstructure is convenient for modeling bone tissue. Its structure is formed by Haversian and Volkmann channels (the primary porosity) and by porous matrix perforated by canaliculi (the dual porosity).

For finite scale $\varepsilon > 0$ domain $\Omega \subset \mathbb{R}^3$ is decomposed into two principal nonoverlapping parts, the channels Ω_c^ε and the matrix Ω_m^ε, so that $\Omega = \Omega_m^\varepsilon \cup \Omega_c^\varepsilon \cup \Gamma_{mc}^\varepsilon$, $\Gamma_{mc}^\varepsilon = \overline{\Omega_m^\varepsilon} \cap \overline{\Omega_c^\varepsilon}$ is the channel-matrix interface. Domain Ω is generated as a periodic lattice using a representative periodic cell $Y = Y_c \cup Y_m \cup \Gamma$, see Fig. 8 (right), where Y_c generating Ω_c^ε represent the channels of the primary porosity separated from the matrix $Y_m = Y \setminus \overline{Y_c}$ by interface Γ.

The model of the homogenized bone tissue is obtained using the Biot model (19). Following the double-porosity ansatz, the permeability $\boldsymbol{K}^\varepsilon$ is scaled by ε^2 in the dual porosity represented by Y_m, namely using the unfolding operator $\mathcal{T}_\varepsilon(\boldsymbol{K}^\varepsilon(x)) = \varepsilon^2 \chi_m(y) \boldsymbol{K}^m(y) + \chi_c(y)\boldsymbol{K}^c(y)$ with $y \in Y$, $x \in \Omega$, where χ_d, $d = m, c$ is the characteristic function of domain Y_d.

Formulation of the macroscopic problem.   The homogenized equations involve stationary and non-stationary homogenized coefficients which serve as convolution kernels and, thus, are responsible for the fading memory effects. These effects are induced by microflows in the dual porosity, due to the fluid-structure interaction at the microscopic level.

In order to compute the homogenized coefficients, microscopic problems must be solved, so that the characteristic responses of the computational cell Y are obtained, see Fig. 9.

All details upon derivation of the homogenized equations can be found in [25]. The
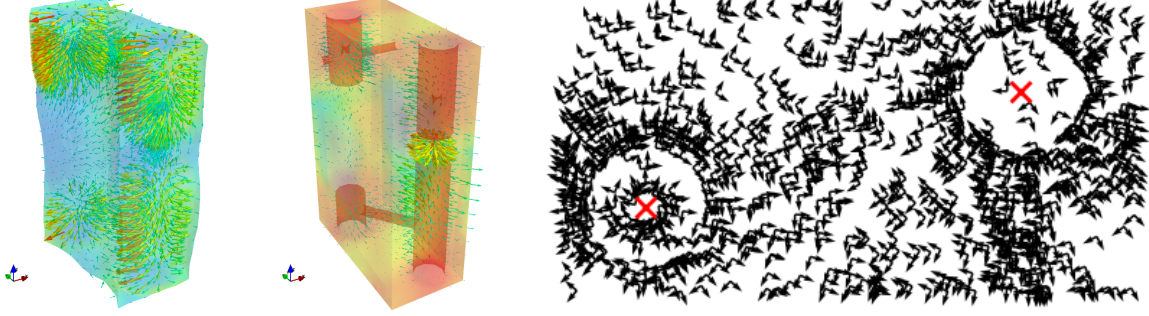
Figure 9: Characteristic response in the reference cell Y – illustration of corrector basis functions (left) and anisotropy of the permeability in the dual porosity (right).

macroscopic problem can be presented in the weak form: for a.a. $t \in]0, T[$ find couple $(\boldsymbol{u}(t, \cdot), p(t, \cdot)) \in V \times H^1(\Omega)$ ($V \subset \mathbf{H}^1(\Omega)$ is determined by kinematic boundary conditions) with initial condition $p(0, \cdot) = 0$, such that

$$
\int_\Omega \mathcal{E}_{ijkl} e_{kl}(\boldsymbol{u}) e_{ij}(\boldsymbol{v}) + \int_\Omega \int_0^t \mathcal{H}_{ijkl}(t-\tau) e_{kl}(\frac{\mathrm{d}}{\mathrm{d}\tau} \boldsymbol{u}(\tau)) \, d\tau \, e_{ij}(\boldsymbol{v})
$$

$$
- \int_\Omega (\mathcal{B}_{ij} + \mathcal{P}_{ij}(0)) \, p \, e_{ij}(\boldsymbol{v}) - \int_\Omega \int_0^t \frac{\mathrm{d}}{\mathrm{d}t} \mathcal{P}_{ij}(t-\tau) p(\tau) \, d\tau \, e_{ij}(\boldsymbol{v}) = \int_{\partial_\sigma \Omega} \boldsymbol{g} \cdot \boldsymbol{v} \, d\Gamma ,
$$

(21)

$$
\int_\Omega (\mathcal{B}_{ij} + \mathcal{P}_{ij}(0)) \, e_{ij}(\frac{\mathrm{d}}{\mathrm{d}t} \boldsymbol{u}) \, q + \int_\Omega \int_0^t \frac{\mathrm{d}}{\mathrm{d}t} \mathcal{P}_{ij}(t-\tau) e_{ij}(\frac{\mathrm{d}}{\mathrm{d}\tau} \boldsymbol{u}(\tau)) \, d\tau \, q
$$

$$
+ \int_\Omega \mathcal{C}_{ij} \partial_j p \partial_i q + \int_\Omega q \mathcal{M} \frac{\mathrm{d}}{\mathrm{d}t} p + \int_\Omega q \int_0^t \mathcal{N}(t-\tau) \frac{\mathrm{d}}{\mathrm{d}\tau} p(\tau) \, d\tau = 0 ,
$$

for all $\boldsymbol{v} \in V_0$ and $q \in H^1(\Omega)$.

Model (21) was implemented numerically, details on the FE discretization and evaluation of the convolution integrals can be found in [15].

3.2.2 Three compartment topology

In perfused tissues the three compartments correspond to two systems of channels (the arterial and venous sectors) separated by the matrix representing the tissue penetrated by capillaries which form the dual porosity.

In analogy with the two-compartment model, for finite scale $\varepsilon > 0$ domain $\Omega \subset \mathbb{R}^3$ is decomposed into three principal nonoverlapping parts, the channels $\Omega_\alpha^\varepsilon$, $\alpha = 1, 2$ and the matrix Ω_3^ε, so that $\Omega = \bigcup_{i=1,2,3} \Omega_i^\varepsilon \cup \Gamma_{23}^\varepsilon \cup \Gamma_{13}^\varepsilon$, where $\Gamma_{\alpha 3}^\varepsilon$ are the channel-matrix interfaces. The reference cell Y is decomposed accordingly: the channels are represented by Y_1 and Y_2 which are mutually disjoint, i.e. $Y_1 \cap Y_2 = \emptyset$, being separated by $Y_3 = Y \setminus \bigcup_{\alpha=1,2} \overline{Y_\alpha}$. Obviously, domain Ω_3^ε is connected.
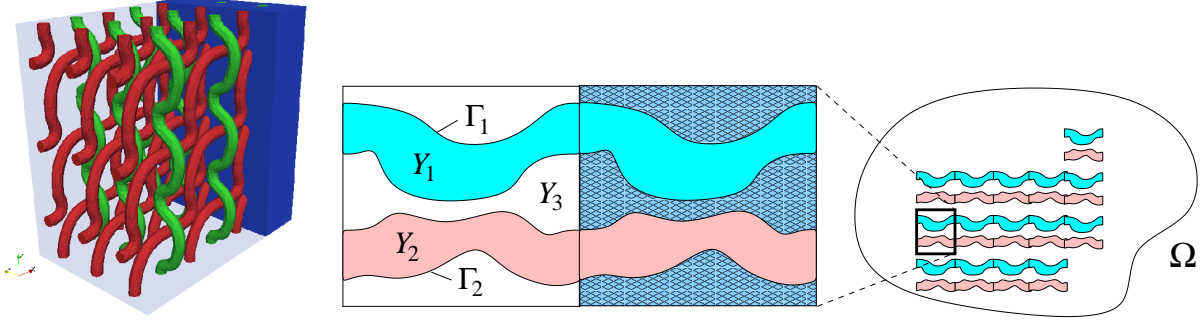
Figure 10: Left: a three-compartment periodic structure, Right: the scheme of the microstructure decomposition.

The homogenization procedure [12, 16] is applied to the Biot model (19) with the incompressibility constraints, which yields $\boldsymbol{\alpha} = 0$ and $1/\mu = 0$. By virtue of the double-porosity ansatz, the permeability $\boldsymbol{K}^\varepsilon$ is scaled by ε^2 in the dual porosity represented by Y_3, so that using the unfolding operator $\mathcal{T}_\varepsilon\big(K_{ij}^\varepsilon(x)\big) = \varepsilon^2 \chi_3(y) K_{ij}^3(y) + \sum_{\alpha=1,2} \chi_\alpha(y) K_{ij}^\alpha(y)$, $y \in Y$, $x \in \Omega$.

As the result of the homogenization, a two-scale system of equations is obtained. Using the Laplace transformation, the two-scale problem is decoupled: *the local microscopic problems* are solved in reference cell Y to obtain the characteristic responses. Consequently, the homogenized coefficients involved in the macroscopic problem can be evaluated.

Local microscopic problems. Besides the steady-state correctors, the time-variant corrector basis functions are defined. For brevity, we introduce the following general form of the local evolutionary problems (see [16]): Find $(\tilde{\boldsymbol{\omega}}(t,y), \tilde{\pi}(t,y))$ such that $\tilde{\boldsymbol{\omega}}(t,\cdot) \in \mathbf{H}_\#^1(Y)$ and $\tilde{\pi}(t,\cdot) \in H_{\#0}^1(Y_3)$ satisfy the following identities for $t > 0$ (the space $H_{\#0}^1(Y_3) \subset H_\#^1(Y)$ contains functions with zero trace on the matrix-channel interfaces $\Gamma_{2,3}$):

$$\int_Y [\boldsymbol{I\!D}(y)\boldsymbol{e}_y(\tilde{\boldsymbol{\omega}}(t,y))] : \boldsymbol{e}_y(\boldsymbol{v}) - \int_{Y_3} \frac{\mathrm{d}}{\mathrm{d}\,t}\tilde{\pi}(t,y)\mathrm{div}_y\boldsymbol{v} = 0 \quad \forall \boldsymbol{v} \in \mathbf{H}_\#^1(Y) \,,$$

$$\int_{Y_3} \psi \mathrm{div}_y \tilde{\boldsymbol{\omega}}(t,y) + \int_Y [\boldsymbol{K}^3 \nabla_y \tilde{\pi}(t,y)] \cdot \nabla_y \psi = g(\psi) \quad \forall \psi \in H_{\#0}^1(Y_3) \,,$$

(22)

where functional $g(\psi)$ and the initial condition on $\tilde{\pi}(0,\cdot)$ is specified. Actually, this generic problem is identified for two cases: local problems for computing strain-associated correctors, $(\tilde{\boldsymbol{\omega}}^{rs}, \tilde{\pi}^{rs})$, and those which are related to channel pressures, $(\tilde{\boldsymbol{\omega}}^\alpha, \tilde{\pi}^\alpha)$.

Homogenized coefficients are evaluated using the corrector basis functions. They express an "integral" form microstructural responses driven by the macroscopic quantities.

- $\mathcal{E}_{ijkl}$ is the elasticity tensor. It expresses the overall elasticity (stiffness) of the dried porous skeleton represented by domain Y, thus, including both the porosities.

- $\mathcal{H}_{ijkl}(t)$ is the viscosity tensor related to the macroscopic creep and relaxation phenomena; it expresses the microflow (perfusion) in the dual porosity Y_3.

- $\mathcal{R}^1_{ij}(t)$ and $\bar{\mathcal{P}}^1_{ij}$ are the poroelastic coefficients which reflect two phenomena: the elasticity of the dried skeleton in Y and permeability of the dual porosity.

- $\tilde{\mathcal{G}}_+(t)$ and $\mathcal{G}^*$ are the perfusion coefficients which control the amount of the fluid exchange between sectors Y_1 and Y_2.

- $\mathcal{C}^\alpha_{ij}$ is the homogenized permeability of the primary porosity in Y_α.

Macroscopic perfusion model describes parallel flows through the two channel systems in deforming medium. The macroscopic displacement field, $\boldsymbol{u}^0(t, \cdot) \in \boldsymbol{V} \subset \mathbf{H}^1(\Omega)$, and the two macroscopic pressures, $p_1(t, \cdot), p_2(t, \cdot) \in H^1_0(\Omega)$ satisfy the equilibrium equation (compare with the two-compartment model (21))

$$\int_\Omega \left[\mathcal{E}_{ijkl} e^x_{kl}(\boldsymbol{u}^0(t, \cdot)) + \int_0^t \mathcal{H}_{ijkl}(t - \tau) \frac{\mathrm{d}}{\mathrm{d}\tau} e^x_{kl}(\boldsymbol{u}(\tau, \cdot)) \, d\tau \right] e^x_{ij}(\boldsymbol{v})$$
$$- \int_\Omega e^x_{ij}(\boldsymbol{v}) \int_0^t \tilde{\mathcal{R}}^1_{ij}(t - \tau)[p_1(\tau, \cdot) - p_2(\tau, \cdot)] \, d\tau \tag{23}$$
$$- \sum_{\alpha=1,2} \int_\Omega \left[\frac{|Y_\alpha|}{|Y|} \delta_{ij} + \bar{\mathcal{P}}^\alpha_{ij} \right] p_\alpha(t, \cdot) \, e^x_{ij}(\boldsymbol{v}) = \int_{\partial_\sigma \Omega} \boldsymbol{g} \cdot \boldsymbol{v} \, dS \quad \forall \boldsymbol{v} \in \boldsymbol{V}_0 \, ,$$

and the two balance-of-mass equations for $\alpha, \beta = 1, 2, \ \beta \neq \alpha$

$$\int_\Omega \mathcal{C}^\alpha_{ij} \partial^x_j p_\alpha(t, \cdot) \partial^x_i q + \int_\Omega q \, \mathcal{G}^* \frac{\mathrm{d}}{\mathrm{d}t} (p_\alpha(t, \cdot) - p_\beta(t, \cdot))$$
$$+ \int_\Omega q \int_0^t \tilde{\mathcal{G}}_+(t - \tau) \frac{\mathrm{d}}{\mathrm{d}\tau} (p_\alpha(\tau, \cdot) - p_\beta(\tau, \cdot)) \, d\tau$$
$$+ \int_\Omega q \int_0^t \tilde{\mathcal{R}}^\alpha_{ij}(t - \tau) \frac{\mathrm{d}}{\mathrm{d}\tau} e^x_{ij}(\boldsymbol{u}^0(\tau, \cdot)) \, d\tau \tag{24}$$
$$+ \int_\Omega q \left[\frac{|Y_\alpha|}{|Y|} \delta_{ij} + \bar{\mathcal{P}}^\alpha_{ij} \right] \frac{\mathrm{d}}{\mathrm{d}t} e^x_{ij}(\boldsymbol{u}^0(t, \cdot)) = 0 \, , \quad \forall q \in H^1_0(\Omega) \, ,$$

which govern the fluid flows in the two channels and its redistribution between them. The terms involving the pressure difference $p_\alpha - p_\beta$ reveal the amount of perfused fluid; while coefficient $\mathcal{G}^*$ is related to transition effects, the perfusion in a steady state is determined by the convolution term involving $\tilde{\mathcal{G}}_+(t - \tau)$, since $\tilde{\mathcal{G}}_+(+\infty) > 0$.

The three-compartment two-scale model was implemented in the **SfePy** FE code [2]. As an example, in Fig. 11 the pressure and perfusion velocities are displayed for a deforming block of tissue with microstructure similar to that of Fig. 10, right.
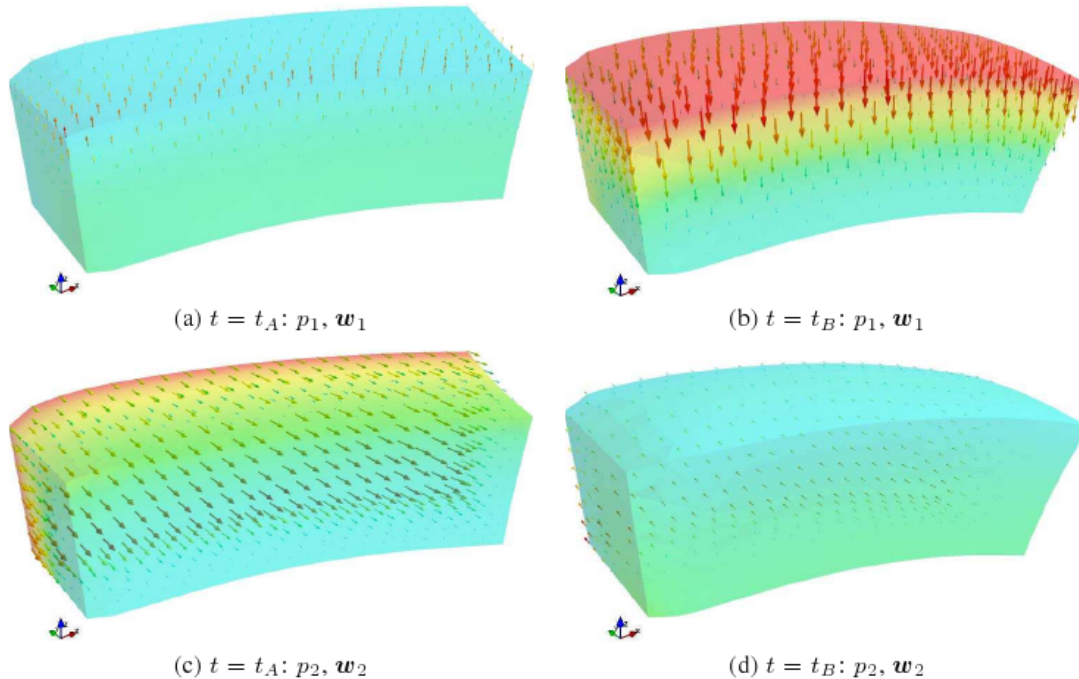
Figure 11: Deformed perfused block: macroscopic pressures p_1 and p_2 displayed by color map at time $t_A = 60\,\text{s}$, (a), (c) and $t_B = 80\,\text{s}$, (b), (d), the associated perfusion velocities are indicated by arrows. Deformation enlarged for visualization. (Computed by R. Cimrman, 2009)

3.3   Large deforming FSPM and linearization

Homogenization of nonlinear partial differential equations is quite cumbersome, in general. The theoretical results, if any, are derived in a generalized frameworks, like the G- or Γ-convergence, [Bra02]. In any case, it is not possible to decouple the scales in terms of a multiplicative decomposition based on the "autonomous characteristic responses" of microstructures.

An alternative approach to treat the nonlinear problems is based on homogenization of linear subproblems arising from an incremental numerical solving procedure, see [10, 11, 17, 8]. The homogenization procedure can be described by the following steps:

- A reference configuration at time t is considered (the time can be artificial, associated with iterations of solving the nonlinear problem). The configuration is defined by locally periodic structure and by the reference state in the form of bounded two-scale functions.

- The homogenization is applied to the linear subproblem: given the configuration at time t, compute the increments associated with time increment Δt. The locally periodic microstructure and the reference state define the oscillating coefficients of

22

the linearized equations. Then the standard homogenization is applied, such that on solving local microscopic problems, the characteristic responses (corrector basis functions) are obtained and the homogenized coefficients are evaluated at any "macroscopic position" x.

- The homogenized subproblem is solved at the macroscopic level, thus the increments of the macroscopic response are obtained.

- In order to establish new microscopic configurations at time $t + \Delta t$ and at "any" macroscopic position, the macroscopic response is combined with the local microscopic characteristic responses to update the local microscopic states. Then the next time step can be considered and the whole procedure repeats.

In contrast with linear problems, where the microscopic responses are solved only once, in nonlinear problems the local microscopic problems must be solved for any iteration (time step) and at "any" macroscopic point, *cf.* [11, 17, 8]. In fact, the homogenization leads to a two-scale domain decomposition: the macroscopic domain is represented locally by "microscopic" cells where the microscopic problems must be solved. The data (i.e. the solutions) are passed between the two levels after any iteration (the time increment step), so that the two-scale problem remains tightly coupled during the whole solution procedure. This is the major difficulty which affects directly the complexity of the numerical treatment.

3.3.1 Incremental formulation

We consider the subproblem of computing the new configuration at time $t + \Delta t$, given a finite time step Δt and the configuration $\mathcal{C}^{\varepsilon,(t)}$ at time t, which is determined by the triplet $\{\Omega, F_{ij}^\varepsilon(x), p^\varepsilon(x)\}(t)$ for $x \in \Omega$, i.e. we write $\mathcal{C}^{\varepsilon,(t)} = \{\Omega, F_{ij}^\varepsilon, p^\varepsilon\}(t)$, where F_{ij}^ε is the deformation gradient, $J^\varepsilon = \det F_{ij}^\varepsilon$, and p^ε is the interstitial fluid pressure.

Let $L^{\text{new}}(\boldsymbol{v})$ be the functional involving the instantaneous boundary and volume forces at time $t + \Delta t$. The finite increments of displacement $\Delta \boldsymbol{u}^\varepsilon \in \boldsymbol{V}_0(\Omega)$ and hydrostatic pressure $\Delta p^\varepsilon \in L^2(\Omega)$ verify the variational equations (25)-(26) which express respectively the balance of stresses – quasi-static equilibrium equation (notation: $\boldsymbol{I} = \delta_{ij}$, $\mathbb{I} = 1/2(\delta_{ik}\delta_{jl} + \delta_{il}\delta_{jk})$, $\eta_{ij}(\boldsymbol{v}) = (\partial v_k/\partial x_i)(\partial v_k/\partial x_j)$)

$$\int_\Omega [\mathbb{D}^{\text{eff},\varepsilon} : \boldsymbol{e}(\Delta\boldsymbol{u}^\varepsilon)] : \boldsymbol{e}(\boldsymbol{v}^\varepsilon)(J^\varepsilon)^{-1}\mathrm{d}x + \int_\Omega \boldsymbol{\tau}^{\text{eff},\varepsilon} : \delta\boldsymbol{\eta}(\Delta\boldsymbol{u}^\varepsilon; \boldsymbol{v}^\varepsilon)(J^\varepsilon)^{-1}\mathrm{d}x$$

$$- \int_\Omega \Delta p^\varepsilon \operatorname{div}\boldsymbol{v}^\varepsilon\mathrm{d}x + \int_\Omega p^\varepsilon \nabla(\Delta\boldsymbol{u}^\varepsilon) : (\mathbb{I} - \boldsymbol{I} \otimes \boldsymbol{I}) : \nabla\boldsymbol{v}^\varepsilon\mathrm{d}x =$$

$$L(\boldsymbol{v}^\varepsilon) - \int_\Omega \boldsymbol{\tau}^\varepsilon : \boldsymbol{e}(\boldsymbol{v}^\varepsilon)(J^\varepsilon)^{-1}\mathrm{d}x \qquad \forall \boldsymbol{v}^\varepsilon \in V(\Omega)\,, \tag{25}$$

and the Darcy flow in the dual-porous structure

$$\int_\Omega q^\varepsilon \operatorname{div}\Delta\boldsymbol{u}^\varepsilon\mathrm{d}x + \Delta t \int_\Omega \boldsymbol{K}^\varepsilon \cdot \nabla(p^\varepsilon + \Delta p^\varepsilon) \cdot \nabla q^\varepsilon\mathrm{d}x = 0\,, \quad \forall q^\varepsilon \in H^1(\Omega)\,. \tag{26}$$

Above the total Kirchhoff stress τ_{ij}^ε is defined as follows:

$$\tau_{ij}^\varepsilon = -J^\varepsilon \delta_{ij}\ p^\varepsilon + \tau_{ij}^{\text{eff},\varepsilon}\ ,\ \text{where}\ \tau_{ij}^{\text{eff},\varepsilon} = \mu^\varepsilon (J^\varepsilon)^{-2/3}\ \text{dev}(F_{ik}^\varepsilon F_{jk}^\varepsilon)\ . \tag{27}$$

We assume the same kind of heterogeneous media, as described in Section 3.2.2, thus involving 3 compartments (represented by the reference cell decomposition $Y = Y_1 \cup Y_2 \cup Y_3$), whereby the dual porosity is associated with Y_3.

3.3.2   Macroscopic equations of the homogenized incremental problem

Given the local microscopic configurations $\mathcal{C}^{(t)}(x)$, the microscopic responses are solved for time increment Δt. Using these responses, the homogenized coefficients $A_{ijkl}, B_{ij}, G_\alpha^\beta, C_{ij}^\beta, Q_{ij}$ and the stress S_{ij} are computed, which constitute the equations of the macroscopic incremental problem: find displacements $\Delta \boldsymbol{u}^0 \in \boldsymbol{V}(\Omega)$ and pressures $\Delta p_\beta^0 \in H^1(\Omega)$, $\beta = 1, 2$ which satisfy:

Equilibrium equation:

$$\int_\Omega \left(A_{ijkl}\partial_l \Delta u_k^0 - \sum_{\alpha=1,2} B_{ij}^\alpha \Delta p_\alpha^0 \right) \partial_j v_i^0 \mathrm{d}x = L(\boldsymbol{v}^0) - \int_\Omega (Q_{ij} + S_{ij})\, \partial_j v_i^0 \mathrm{d}x \tag{28}$$

for all $\boldsymbol{v}^0 \in \boldsymbol{V}_0(\Omega)$,

Diffusion equations: for $\beta = 1, 2$,

$$\int_\Omega q_\beta^0 \left(B_{ij}^\beta \partial_j \Delta u_i^0 + \sum_{\alpha=1,2} G_\alpha^\beta \Delta p_\alpha^0 \right) \mathrm{d}x + \int_\Omega C_{kl}^\beta \partial_l (\Delta p_\beta^0 + p_\beta^0)\, \partial_k q_\beta^0 \mathrm{d}x = -\int_\Omega g_\beta^{\text{eff}} q_\beta^0 \mathrm{d}x\ , \tag{29}$$

for all $q_\beta^0 \in H^1(\Omega)$.

It is worth noting that the homogenized problem involves two diffusion equations describing perfusion in the two compartments labeled by $\beta = 1, 2$. This is the direct consequence of a) the dual porosity in Y_3 and b) topology of the decomposition of Y with Y_1 disconnected from Y_2.

Upon computing the macroscopic increments, the local microscopic configurations must be updated, to continue the time stepping algorithm for the next time increment. At a certain time level, which is referred to by superscript (t), the macroscopic configuration is represented by the triplet $\mathcal{M}^{(t)} \equiv \{\Omega^{(t)}, F_{ij}^{(t)}(x), p_\alpha^{(t)}(x)|\ x \in \Omega^{(t)}\}$ and the microscopic configurations $\mathcal{C}^{(t)}(x)$ are defined by deformations and pressure in local cell $Y(x)$.

3.4 Homogenization of perfusion in thin layers

Homogenization can be adapted also for structures where the periodicity is restricted to directions within a given plane, as pointed out in Section 2.3.

In paper [14] we derived a homogenized model of the Darcy flow in a thin porous non-deformable layer. The reference periodic cell is composed of the matrix representing the dual porosity and of two mutually disconnected channels representing the primary porosity. The resulting model describes macroscopic redistribution of the fluid in the plane to which the thin layer is reduced. Thus, a 3D block of a given heterogeneous body can be replaced by a finite number of the homogenized layers, being supplemented by coupling conditions that govern the fluid exchange between the adjacent layers.

One of the promising applications of the model is the blood perfusion in the brain tissue, see Fig. 12 (left). Although a detailed morphological study is not completed yet, the following assumptions, however simplifying, seem to be relevant:

- change of the microstructure with the depth in the tissue (the radial direction), as indicated by two layers,

- repeated patterns of the microstructure with respect to the tangential direction, so that the periodic "artificial" lattice can be introduced.

One of the main difficulties of modeling the blood perfusion is inherited form the structure of the vascular system. Although its features are specific for different types of tissues, in general, the vasculature forms a *complex hierarchical structure* represented by a branching network. It consists of several *levels* distinguishable according to the vessel diameter. On one hand, homogenization is well suited for describing periodic structures, so it does not conform with the branching structures. On the other hand, the "ideal perfusion tree" can be decomposed into several levels (hierarchies) which can be associated with layers (generated by curved "mean" surfaces); in each of them the vascular network can be approximated by a (locally) periodic structures, where the "plane periodicity" is related to the tangent planes of the generating surface. This simplified view of the real complex system give rise to the idea of decomposing a 3D volume into layers with a given periodic structure, see Fig. 12 (right), so that the homogenization procedure can be applied.

3.4.1 Problem formulation

Homogenization of the perfusion problem in a heterogeneous layer with double porosity was described in [14]. In Fig. 12 (right) the layer is depicted schematically: Layer $\Omega^\delta = \Gamma_0 \times] - \delta/2, +\delta/2[$ has thickness $\delta > 0$, whereby $\Gamma_0 \subset \mathbb{R}^2$ forms the mean surface. On the "upper" and "lower" boundaries of Ω^δ, which are denoted by $\Gamma^{\delta+}$ and $\Gamma^{\delta-}$, the fluid exchange with the outer space is controlled by Neumann conditions. Domain Ω^δ consists of three disjoint sectors, the matrix $\Omega_M^{\varepsilon\delta}$ and the two channels $\Omega_A^{\varepsilon\delta}$, $\Omega_B^{\varepsilon\delta}$, which are generated as periodic lattices (with period ε). The double porosity in the matrix $\Omega_M^{\varepsilon\delta}$ is introduced using the standard scaling ansatz for the permeability, as described in preceding sections.
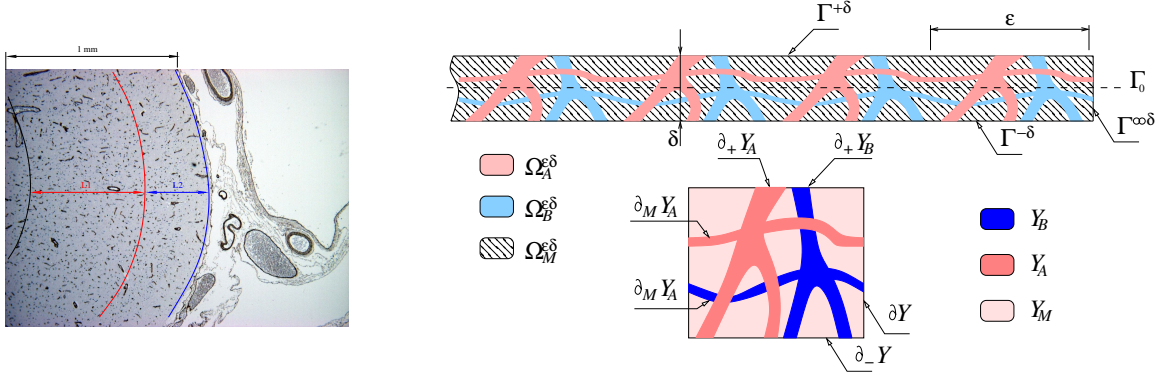
Figure 12: Left: Brain tissue and micro-vessels. The microstructure changes with the depth and can be decomposed into layers. Right: The three compartment heterogeneous layer and the domain and boundary decomposition of the reference periodic cell Y.

Dilated formulation. For homogenization, the perfusion problem is transformed on dilated domain with unit thickness; the weak formulation reads as follows: For given fluxes $g^{\varepsilon\pm} \in L^2(\Gamma^\pm)$, find $p^\varepsilon \in H^1(\Omega)/\mathbb{R}$ such that

$$\sum_{D=A,B} \int_{\Omega_D^\varepsilon} \nabla q \cdot \boldsymbol{K}^\varepsilon \cdot \nabla p^\varepsilon + \int_{\Omega_M^\varepsilon} \nabla q \cdot \varepsilon^2 \bar{\boldsymbol{\kappa}}^\varepsilon \cdot \nabla p^\varepsilon = \frac{1}{\delta} \int_{\Gamma^+ \cup \Gamma^-} g^{\pm\varepsilon} q \, \mathrm{dS}_x \quad \forall q \in H^1(\Omega) \,. \tag{30}$$

In order to obtain a limit of problem (30), the perfusion fluxes $g^{\pm\varepsilon}$ must be scaled properly w.r.t. ε: we assume that the fluxes through the matrix interface $\Gamma_M^{\pm\varepsilon}$ are of the order ε, whereas fluxes of the channel inlets and outlets are of the order 1. Moreover, local net source of channels A and B must be specified. For this we introduce $G_D^\varepsilon(x')$, $x' \in \Gamma_0$, with $D = A, B$, to describe the fluid volume increase per one period ε in the channel compartment D, and assume $G_D^\varepsilon \sim \varepsilon$, i.e. the local source produced in the channel A, or B due to external inlets/outlets is proportional to the thickness $\delta = h\varepsilon$ of the layer.

3.4.2 Model of the homogenized layer

The microscopic problems are solved in the reference cell Y decomposed into domains Y_A, Y_B representing the channels A and B, respectively, and into the matrix Y_M featured by the dual porosity. The channels have inlet / outlet branches which "intersect" the layer faces Γ^+, Γ^- at "inlet / outlet surfaces" denoted as $\mathcal{A}_D^k$ and labeled by indices $k \in J_D$.

In the limit, two "macroscopic" pressures $p^{0,A}$ and $p^{0,B}$ are obtained associated with channels A and B. The dimension of the problem is reduced from 3D to 2D. The problem describes the fluid redistribution in Γ_0 due to the following phenomena:

- the macroscopic Darcy flow associated with pressure gradients $\partial_\alpha p^{0,A}, \partial_\alpha p^{0,B}$ and corresponding *in-plane permeabilities* $\mathcal{K}_{\alpha\beta}^A$, $\mathcal{K}_{\alpha\beta}^B$ of channels A,B, where $\alpha, \beta = 1, 2$ are indices of the in-plane coordinates;

26

$p^{0,D}$	macroscopic pressure in channel D		
$\hat{g}^+, \hat{g}^-$	inlet / outlet fluxes of the dual porosity through $\Gamma^{+/-}$		
$\tilde{g}_D^k$	inlet / outlet fluxes of channel D through $\mathcal{A}_D^k$		
$\bar{G}_D$	limit of the channel source flux G_D^ε		

range of indices: $D = A, B, \quad k \in J_D, \quad \alpha, \beta = 1, 2$

notation	description	corrector function defining the coeff.	related function in equations (31)
$\mathcal{K}_{\alpha\beta}^D$	in-plane permeability	π_D^α	$\partial_\beta p^{0,D}$
$\mathcal{G}$	perfusion coefficients	η_D	$p^{0,A} - p^{0,B}$
$\mathcal{F}^{D+}, \mathcal{F}^{D-}$	matrix drainage coefficients	γ^+, γ^-	$\hat{g}^+, \hat{g}^-$
$\mathcal{S}_\alpha^{D,k}$	channel branch drainage-saturation	γ_D^k	$\tilde{g}_A^k$

Table 1: Variables and coefficients involved in the model of the homogenized perfused layer.

- the local fluid exchange between channels A and B through the dual porosity, where the amount of the fluid is proportional to $p^{0,A} - p^{0,B}$ with perfusion coefficient $\mathcal{G}$;

- the external fluxes through the layer interfaces; in Table 1 we introduce the notation for these homogenized fluxes (obtained as limits of $g^{+,\varepsilon}$ and $g^{-,\varepsilon}$) and for associated homogenized coefficients. The limit fluxes associated with channels D are $\tilde{g}_D^\pm$ and $\bar{G}_D$; it can be shown that $\tilde{g}_D^\pm$, since $\bar{G}_D^\varepsilon \approx \varepsilon$.

Perfusion in the homogenized layer is governed by the following two equations, each per one channel system (the summation convention applies in indices α, β)

$$
-\frac{\partial}{\partial x_\alpha} \left[\mathcal{K}_{\alpha\beta}^A \frac{\partial}{\partial x_\beta} p^{0,A} + \sum_{k \in J_A} \mathcal{S}_\alpha^{A,k} \tilde{g}_A^k \right] + \mathcal{G} \left(p^{0,A} - p^{0,B} \right)
$$
$$
= \frac{|\partial Y_A^\pm|}{h} \bar{G}_A - \mathcal{F}^{A+} \hat{g}^+ - \mathcal{F}^{A-} \hat{g}^- \qquad \text{in } \Gamma_0 \, ,
$$

$$
-\frac{\partial}{\partial x_\alpha} \left[\mathcal{K}_{\alpha\beta}^B \frac{\partial}{\partial x_\beta} p^{0,B} + \sum_{k \in J_B} \mathcal{S}_\alpha^{B,k} \tilde{g}_B^k \right] + \mathcal{G} \left(p^{0,B} - p^{0,A} \right)
$$
$$
= \frac{|\partial Y_A^\pm|}{h} \bar{G}_B - \mathcal{F}^{B+} \hat{g}^+ - \mathcal{F}^{B-} \hat{g}^- \qquad \text{in } \Gamma_0 \, ,
$$

(31)

Boundary $\partial\Gamma_0$ is impermeable, so that fluxes $\hat{g}^{+/-}, \bar{G}_D$ and $\tilde{g}_D^k$ are given data and must
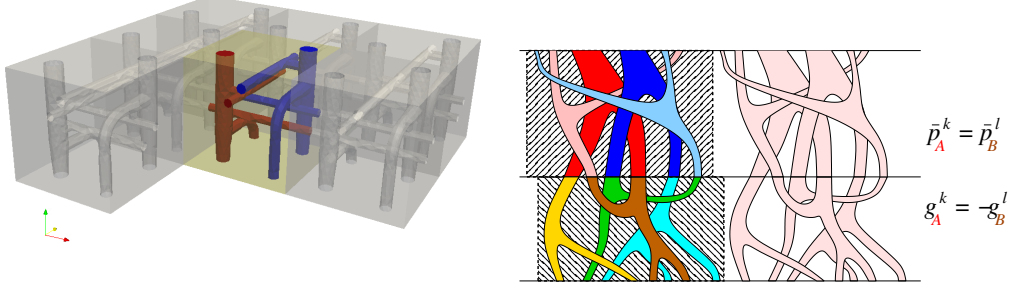
Figure 13: Left: Representative periodic cell of the layer containing two systems channels. Right: illustration of the perfusion tree and a possible decomposition into layers.
.

satisfy the solvability conditions:

$$
\sum_{k \in J_D} |\mathcal{A}_D^k| \tilde{g}_D^k = 0, \quad D = A, B , \quad \text{and} \quad \sum_{D=A,B} \int_{\Gamma_0} \left(\frac{1}{h} \bar{G}_D + \mathcal{F}^{D+} \hat{g}^+ + \mathcal{F}^{D-} \hat{g}^- \right) = 0 . \quad (32)
$$

Model extension – perfusion tree. To summarize, let's recall the need for describing perfusion in tree-like structures which can be considered as periodic at any level of the "tree". In this context, the following properties are important.

- *Multiple channels.* Model (31) can be generalized for more mutually disjoint channels, whereby the same techniques (also for the proofs of a priori estimates) can be used, see [14] for details.

- *Multiple layers.* The main idea of using the homogenization-based modeling of the "tree" is to decompose a 3D continuum occupying a thick heterogeneous layer into a certain number of "thin" layers described by model (31). Thus, we obtain a coupled system of 2D models describing the perfusion in the double porous medium.

- *Co-lateral channels and blood perfusion.* Model (31) has been justified only for the case when "co-lateral" channels exist, i.e. domain Ω_D^ε, $D = A, B$ is connected, which yields positive definite tensor $\mathcal{K}^D$. For disconnected domains a rigorous proof is to be completed, however, model (31) can be adapted for this situation and make a sense when multiple coupled layers are considered. Let us remark that in some tissues, co-lateral channels are not well developed (in brain), besides pathological cases.

The coupling conditions can be introduced in several ways, although we consider the simplest and the most obvious case: the interface between the layers is just a section through heterogeneous structure with well defined decomposition into the channels and the matrix, see an illustration in Fig. 13, right.
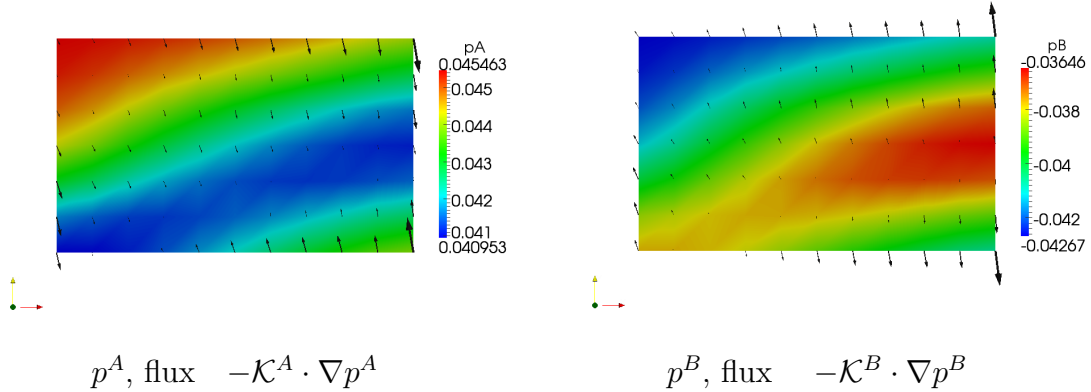
28

p^A, flux $\quad -\mathcal{K}^A \cdot \nabla p^A$ $\qquad\qquad\qquad$ p^B, flux $\quad -\mathcal{K}^B \cdot \nabla p^B$

Figure 14: Solutions of the macroscopic problem: macroscopic pressures and fluxes in Γ_0.

3.4.3 Numerical illustration

The homogenized single layer model is implemented in code **SfePy** , material coefficients involved in (31) are evaluated for the microstructure of the 3D periodic cell including two channels, see Fig. 13, left. The macroscopic problem is solved for given external fluxes, see Tab. 1, the "macroscopic" solutions p^A, p^B on Γ_0 are illustrated in Fig. 14, where the local amount of the perfused fluid is $\mathcal{G}(p^A - p^B)$. Once the macroscopic pressures are computed, at any point of Γ_0, the fluid pressures and perfusion fluxes can be reconstructed at the microscopic level, see an illustration in Fig. 15.

Literature used , related to Section 2 (selection): [AB92] [AB93] [ADH90] [ASBH90] [BCP03] [Bio55] [CHBA94] [Cow01] [Cri91] [Cri97] [dB00] [dBCD98] [EP02] [FM03] [Fri00] [HC95] [Hol00] [Hor97] [LNR10] [MC96] [MGL01] [Pes96] [SH98] [SM02] [SP80] [SV04] [TIK98] [TOZN00]

4 Appended research papers and the author's contribution

The issues discussed briefly above were published during past five years in research papers which are now listed with short comments. In these papers *numerical computations* were performed in part by E. Rohan using the in-house Matlab code (developed exclusively by him; below the abbreviation **RHM** is used). Contribution of Dr. R. Cimrman and Dr. V. Lukeš is namely in the numerical computations using the **SfePy** software, or another in-house developed codes (in Matlab; below the abbreviation **LHM** is used), see Section 1.1 of the DISSERTATION for details.

- **Piezoelectricity.** In [9] the homogenization of a general piezoelectric composite
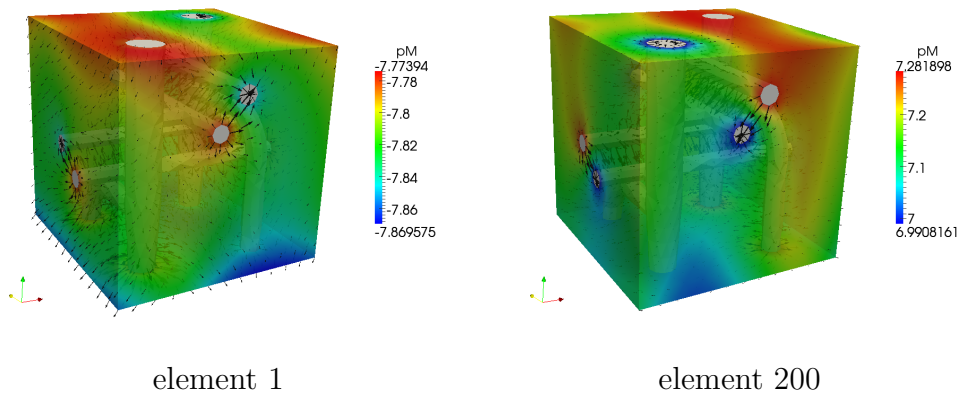
element 1   element 200

Figure 15: Perfusion reconstruction at the microscopic level — pressure $p_M(x', \cdot)$ and perfusion velocities $\boldsymbol{w}_M(x', \cdot)$ in matrix, as evaluated at two different macroscopic points (elements).

with anisotropic elastic inclusions is described, numerical examples of 2D were computed using **RHM** . In [21], the shape sensitivity of the homogenized coefficients was developed, 2D numerical examples discussed (computation using **RHM**). In the context of the *phononic crystals*, the piezoelectric materials were considered in [22], where the sensitivity analysis of the band gaps was developed, and in [3], where the dispersion of guided waves was analyzed numerically using **SfePy** .

- **Phononic crystals.** Homogenization of the phononic crystals is reported in the mathematical paper [1], where the author's contribution is mainly related to numerical examples computed using **RHM** code. In [24], some further modeling aspects were discussed and the dispersion analysis was introduced also for guided waves. The numerical studies performed there using **RHM** code (and using some extensions made by F. Seifrt) indicate the range of applicability of the homogenized model for the band gap prediction. Extensions of modeling the phononic effect in piezoelectric materials were reported in [22] (sensitivity analysis) and in [3] (dispersion of guided waves). More complex phononic structures involving 3 materials were considered in [4]. The sensitivity analysis for the band gap optimization problem was developed in [23] for the "multimodal situations", so that a robust (sub)gradient-based algorithm can be used to solve the problem numerically; there the numerical studies were performed by the author using **RHM** code.

- **Acoustic transmission.** Homogenization of the acoustic waves propagating through thin layer containing the perforated obstacle was developed in [20], where also some numerical illustrative examples were introduced (computations using **LHM** code). The sensitivity analysis with respect to the shape of the periodic perforations was reported in [18] for a general objective function. The numerical implementation is

30

now being developed by V. Lukeš.

- **Linear Biot type medium.** In [5] we discuss homogenization of the incompressible Biot continuum, where the dual porosity has the form of inclusions. In paper [25], see Section 3.2.1, we describe homogenization of compressible double porous Biot type medium with two compartments topology; the dual porosity forms a connected domain (matrix). The numerical issues related to the FEM discretization and treatment of the convolution integrals (fading memory) is discussed in [15] (numerical implementation in the code **SfePy**). This research was motivated by possible applications in bone tissue modeling. In order to describe some effects related to semipermeable interfaces between osteons (the structural units), we studied homogenization of strongly heterogeneous FSPM with discontinuous pressure along microstructural interfaces, see [6].

For modeling tissue perfusion, the three compartment model was developed. The research was published in several proceedings during five years, *cf.* [12], however the first complete paper appeared only recently [16].

- **Large deforming FSPM.** This topic has been motivated by structure of soft tissues, namely by smooth muscles. A large part of the author's habilitation thesis [10] has been devoted to two-scale modeling of large deforming hyperelastic solids with fluid inclusions. In paper [13], the theory was extended for modeling FSPM with a single fluid inclusion per RPC (cell Y). The homogenization is based on the incremental formulation using the updated Lagrangian configuration. It has been demonstrated how the microflow in the dual porosity leads to the apparent viscoelasticity. Numerical examples were performed by the author using the **RHM** program codes. In paper [17] the theory has been extended for description of material with more fluid inclusions in the RPC. For modeling blood perfusion in large deforming tissue, the three compartment model was developed [19].

- **Perfused layers.** In order to cope with blood flows associated with a complex "perfusion tree" characterized by branching vessels, the model of perfusion in layered structures was proposed, see Section 3.4. The theory is explained in [14].

General references

[AB92]   J.-L. Auriault and C. Boutin. Deformable porous media with double porosity. quasi statics. i. coupling effects. *Transp. Porous Media*, 7(1):63–82, 1992.

[AB93]   J.-L. Auriault and C. Boutin. Deformable porous media with double porosity. quasi statics. ii. memory effects. *Transp. Porous Media*, 10(2):153–169, 1993.

[ADH90]   T. Arbogast, J. Douglas, and U. Hornung. Derivation of the double porosity model of single phase flow via homogenization theory. *SIAM J. Math. Anal.*, 21:823–836, 1990.

[AK04]   T. S. Angell and A. Kirsch. *Optimization Methods in Electromagnetic Radiation.* Springer-Verlag, New York, 2004.

[All89]   G. Allaire. Homogenization of the stokes flow in a connected porous medium. *Asymptotic Analysis*, 2:203–222, 1989.

[All92]   G. Allaire. Homogenization and two-scale convergence. *SIAM J. Math. Anal.*, 23:1482–1518, 1992.

[ASBH90]   J. L. Auriault, T. Strzelecki, J. Bauer, and S. He. Porous deformable media saturated by a very compressible fluid: quasi-statics. *European J. Mech. - A/Solids*, 9(4):373–392, 1990.

[BCP03]   A. Bourgeat, G.A. Chechkin, and A.L. Piatnitski. Singular double porosity model. *Applicable Analysis*, 82:103–116, 2003.

[BCZ87]   T. Bourbie, O. Coussy, and B. Zinszner. *Acoustics of porous media.* Techinp, 1987.

[BD94]   A. Bedford and D.S. Drumheller. *Elastic Wave Propagation.* J. Wiley, Chichester, 1994.

[Ben78]   *Asymptotic Analysis for Periodic Structures.* North-Holland, 1978.

[BF04]   G. Bouchitté and D. Felbacq. Homogenization near resonances and artificial magnetism from dielectrics. 1339:377–382, 2004.

[Bio55]   M. A. Biot. Theory of elasticity and consolidation for a porous anisotropic solid. *J. Appl. Phys.*, 26(2):182–185, 1955.

[Bra02]   A. Braides. Γ-*convergence for Beginners, Oxford Lecture Series in Mathematics and its Applications 22.* Oxford University Press, Oxford, 2002.

[CD99]   D. Cioranescu and P. Donato. *An Introduction to Homogenization, Oxford Lecture Series in Mathematics and its Applications 17.* Oxford University Press, Oxford, 1999.

[CDG08]   D. Cioranescu, A. Damlamian, and G. Griso. The periodic unfolding method in homogenization. *SIAM Journal on Mathematical Analysis*, 40(4):1585–1620, 2008.

[CDGO08]   D. Cioranescu, A. Damlamian, G. Griso, and D. Onofrei. The periodic unfolding method for perforated domains and neumann sieve models. *J. Math. Pures Appl.*, 89:248–277, 2008.

[Cea09]   R. Cimrman and et al. SfePy home page. http://sfepy.kme.zcu.cz,http://sfepy.org, 2009. Software, finite element code and applications.

[CHBA94]   D. H. Campen, J. M. Huyghe, P. H. M. Bovendeerd, and T. Arts. Biomechanics of the heart muscle. *Eur. J. Mech., A/Solids*, 13(4):19–41, 1994.

[Cou04]   O. Coussy. *Poromechanics*. John Wiley & Sons, 2004.

[Cow01]   S. C. Cowin. *Bone mechanics handbook*. CRC Press, Boca Raton, FL, 2nd edition, 2001.

[Cri91]   M.A. Crisfield. *Non-linear Finite Element Analysis of Solids and Structures (Essentials)*, volume I. J. Wiley & Sons, Chichester, 1991.

[Cri97]   M.A. Crisfield. *Non-linear Finite Element Analysis of Solids and Structures*, volume II. J. Wiley & Sons, Chichester, 1997.

[CSJP99]   D. Cioranescu and J. Saint Jean Paulin. *Homogenization of Reticulated Structures, Applied Mathematical Sciences 136*. Springer, New York, 1999.

[dB00]   R. de Boer. *Theory of Porous Media*. Springer, Berlin, 2000.

[dBCD98]   P. de Buhan, X. Chateau, and L. Dormieux. The constitutive equations of finite strain poroelasticity in the light of a micro-macro approach. *Eur. J. Mech. A/Solids*, 17:909921, 1998.

[EP02]   H.I. Ene and D. Poliševski. Model of diffusion in partially fissured media. *Z. angew. Math. Phys.*, 53:1052–1059, 2002.

[FM03]   J.L. Ferrín and A. Mikelić. Homogenizing the acoustic properties of a porous matrix containing an incompresssible inviscid fluid. *Math. Meth. Appl. Sci.*, 26:831–859, 2003.

[Fri00]   A.J.H. Frijns. *A four-component theory applied to cartilaginous tissues: numerical modelling and experiments*. PhD thesis, Eindhoven University of Technology, Eindhoven, 2000.

[HC95]   J. M. Huyghe and D. H. Campen. Finite deformation theory of hierarchically arranged porous solids, part i.,ii. *Int. J. Engrg. Sci.*, 33(13):1861–1886, 1995.

[HCK86]   E. J. Haug, K. Choi, and V. Komkov. *Design Sensitivity Analysis of Structural Systems*. Academic Press, Orlando, 1986.

[HM03]   J. Haslinger and R. A. E. Mäkinen. Introduction to shape optimization. *Advances in Design and Control, SIAM*, 2003.

[HN88]   J. Haslinger and P. Neittaanmaki. *Finite Element Approximation for Optimal Shape Design*. J. Wiley, Chichester, 1988.

[Hol00]   G. A. Holzapfel. *Nonlinear Solid Mechanics*. J. Wiley, Chichester, 2000.

[Hor97]   U. Hornung. *Homogenization and porous media*. Springer, Berlin, 1997.

[JP06]   J.S. Jensen and N.L. Pedersen. On maximal eigenfrequency separation in two-material structures: the 1d and 2d scalar cases. *J. Sound Vib.*, 289:967986, 2006.

[LNR10]   T. Lemaire, S. Naili, and A. Rémond. Multi-scale analysis of the coupled effects governing the movement of interstitial fluid in cortical bone. *Biomechan. Model. Mechanobiol.*, 80(6):1289–1301, 2010.

[MC96]   M. A. Murad and J. H. Cushman. Multiscale flow and deformation in hydrophilic swelling media. *Int. Jour. Eng. Sci.*, 34:313–338, 1996.

[MGL01]   A.M. Murad, J.N. Guerreiro, and A.F.D. Loula. Micromechanical computational modelling of secondary consolidation and hereditary creep in soils. *Comput. Methods Appl. Mech. Engrg.*, 190:1985–2016, 2001.

[MT07]   A. Mielke and A. Timofte. Two-scale homogenization for evolutionary variational inequalities via the energetic formulation. *SIAM J. Math. Anal.*, 39:642–668, 2007.

[MW07]   G.W. Milton and J.R. Willis. On modifications of newtons second law and linear continuum elastodynamics. *Proc. R. Soc. A*, 483:855880, 2007.

[NNH]   S. Nemat-Nasser and M. Hori. *Micromechanics: Overall Properties of Heterogeneous Materials*. Series in Applied Mathematics and Mechanics. North-Holland.

[OSY92]   O.A. Oleinic, G.A. Shamaev, and G.A. Yosifian. *Mathematical problems in elasticity and homogenisation*. North Holland, 1992.

[Pes96]   M. Peszynska. Finite element approximation of diffusion equations with convolution terms. *Math. of Comput.*, 65(215):1019–1037, 1996.

[RD00]   D. Royer and E. Dieulesaint. *Elastic Waves in Solids I, Free and Guided Propagation*. Springer, Heidelberg, 2000.

[SH98]   J.C. Simo and T.J.R. Hughes. *Computational Inelasticity*. Springer-Verlag, Berlin, 1998.

[SJ03]   O. Sigmund and J.S. Jensen. ystematic design of phononic band-gap materials and structures by topology optimization. *Phil. Trans. R. Soc. Lond. A*, 361:10011019, 2003.

[SM02]   R.E. Showalter and B. Momken. Single-phase flow in composite poro-elastic media. *Math. Methods Appl. Sci.*, 25:115139, 2002.

[SP80]   E. Sanchez-Palencia. *Non-homogeneous media and vibration theory*. Number 127 in Lecture Notes in Physics. Springer, Berlin, 1980.

[SV04]   R.E. Showalter and D.B. Visarraga. Double-diffusion models from a highly heterogeneous medium. *Journal of Mathematical Analysis and Applications*, 295:191–210, 2004.

[TIK98]   K. Terada, T. Ito, and N. Kikuchi. Characterization of the mechanical behaviors of solid-uid mixture by the homogenization. *Comput. Methods Appl. Mech. Eng.*, 153:223257, 1998.

[TOZN00] N. Takano, Y. Ohnishi, M. Zako, and K. Nishiyabu. The formulation of homogenization method applied to large deformation. *Int. J. Solids Struct.*, 37:65176535, 2000.

[Zv02]   J. Zeman and M. Šejnoha. On determination of periodic unit cell for plain weave fabric composites. *Engineering Mechanics*, 9(1–2):65–74, 2002.

Own works

[1] A. Ávila, G. Griso, B. Miara, and E. Rohan. Multiscale modeling of elastic waves: Theoretical justification and numerical simulation of band gaps. *Multiscale Modeling & Simulation, SIAM*, 7:2008, 1-21.

[2] R. Cimrman and et al. SfePy home page. http://sfepy.kme.zcu.cz,http://sfepy.org, 2009. Software, finite element code and applications.

[3] R. Cimrman and E. Rohan. On acoustic band gaps in homogenized piezoelectric phononic materials. *Appl. Comp. Mech.*, 4:89–100, 2010.

[4] R. Cimrman and E. Rohan. Three-phase phononic materials. *Appl. Comp. Mech.*, 3:2009, 516.

[5] G. Griso and E. Rohan. On the homogenization of a diffusion-deformation problem in strongly heterogeneous media. *Ricerche mat.*, 56:161–188, 2007.

[6] G. Griso and E. Rohan. Homogenization of diffusion-deformation in dual-porous medium with discontinuity interfaces. *SIAM, MMS*, 2010. Submitted.

[7] G. Leugering, E. Rohan, and F. Seifrt. Modeling of metamaterials in wave propagation. In *Chapter in: Wave Propagation in Periodic Media Analysis, Numerical Techniques and practical Applications*. Matthias Ehrhardt (ed.), E-Book Series Progress in Computational Physics,, 2010.

[8] V. Lukeš and E. Rohan. Microstructure based two-scale modelling of soft tissues. *Math. and Computers in Simulation*, 65(215):1019–1037, 1996.

[9] B. Miara, E. Rohan, M. Zidi, and B. Labat. Piezomaterials for bone regeneration design - homogenization approach. *Jour. of the Mech. and Phys. of Solids*, 53:2005, 2529-2556.

[10] E. Rohan. *Mathematical modelling of soft tissues*. Univ. West Bohemia, Pilsen, habilitation thesis edition, 2002.

[11] E. Rohan. Sensitivity strategies in modelling heterogeneous media undergoing finite deformation. *Math. and Computers in Simulation*, 61(3-6):261–270, 2003.

[12] E. Rohan. Homogenization approach to the multi-compartment model of perfusion. *PAMM*, 6:79–82, 2006.

[13] E. Rohan. Modelling large deformation induced microflow in soft biological tissues. *Theor. and Comp. Fluid Dynamics*, 20:251–276, 2006.

[14] E. Rohan. Homogenization of the Darcy flow in a double-porous layer. *SIAM, MMS*, 2010. Submitted.

[15] E. Rohan and R. Cimrman. Multiscale FE simulation of diffusion-deformation processes in homogenized dual-porous media. *Math. Comp. Simul.*, 2009. Submitted.

[16] E. Rohan and R. Cimrman. Two-scale modelling of tissue perfusion problem using homogenization of dual prous media. *Int. Jour. for Multiscale Comput. Engrg.*, 8:81–102, 2010.

[17] E. Rohan, R. Cimrman, and V. Lukeš. Numerical modelling and homogenized constitutive law of large deforming fluid saturated heterogeneous solids. *Computers and Structures*, 84:1095–1114, 2006.

[18] E. Rohan and V. Lukeš. Sensitivity analysis for the optimal perforation problem in acoustic trasmission. *Appl. Comp. Mech.*, 3:111–120, 2009.

[19] E. Rohan and V. Lukeš. Homogenization of perfusion in large-deforming medium using the updated lagrangian formulation. In *Proceedings of the ECT 2010 conference.* Coburg-Sax Publ., 2010.

[20] E. Rohan and V. Lukeš. Homogenization of the acoustic transmission through perforated layer. *J. of Comput. and Appl. Math.*, 6:1876–1885, 2010.

[21] E. Rohan and B. Miara. Homogenization and shape sensitivity of microstructures for design of piezoelectric bio-materials. *Mechanics of Advanced Materials and Structures*, 13:473–485, 2006.

[22] E. Rohan and B. Miara. Sensitivity analysis of acoustic wave propagation in strongly heterogeneous piezoelectric composite. In *Topics on Mathematics for Smart Systems*, pages 139–207. World Sci. Publishing Company, 2006.

[23] E. Rohan and B. Miara. Shape sensitivity analysis for material optimization of homogenized piezo-phononic materials. In *8th World Congress on Structural and Multidisciplinary Optimization.* ECCOMAS, 2009.

[24] E. Rohan, B. Miara, and F. Seifrt. Numerical simulation of acoustic band gaps in homogenized elastic composites. *International Journal of Engineering Science*, 47:2009, 573-594.

[25] E. Rohan, S. Naili, R. Cimrman, and T. Lemaire. Multiscale modelling of a fluid saturated medium with double porosity: relevance to the compact bone. *Submitted*, 2010.